Available online at www.sciencedirect.com

ScienceDirect

Geochimica et Cosmochimica Acta 208 (2017) 63–85

Geochimica et Cosmochimica Acta

www.elsevier.com/locate/gca

Primary magmas and mantle sources of Emeishan basalts constrained from major element, trace element and Pb isotope compositions of olivine-hosted melt inclusions

Zhong-Yuan Ren [a,*], Ya-Dong Wu [a,b], Le Zhang [a,b], Alexander R.L. Nichols [c], Lu-Bing Hong [a], Yin-Hui Zhang [a,b], Yan Zhang [a,b], Jian-Qiang Liu [d], Yi-Gang Xu [a]

[a] *State Key Laboratory of Isotope Geochemistry, Guangzhou Institute of Geochemistry, Chinese Academy of Sciences, Guangzhou 510640, China*
[b] *University of Chinese Academy of Sciences, Beijing 100049, China*
[c] *Research and Development Center for Ocean Drilling Science, Japan Agency for Marine Earth Science and Technology (JMSTEC), 2-5 Natsushima-cho, Yokosuka, Kanagawa 237-0061, Japan*
[d] *State Key Laboratory for Mineral Deposits Research, School of Earth Sciences and Engineering, Nanjing University, 22 Hankou Road, Nanjing 210093, China*

Received 29 October 2015; accepted in revised form 21 January 2017; available online 27 March 2017

Abstract

Olivine-hosted melt inclusions within lava retain important information regarding the lava's primary magma compositions and mantle sources. Thus, they can be used to infer the nature of the mantle sources of large igneous provinces, which is still not well known and of the subject of debate. We have analysed the chemical compositions and Pb isotopic ratios of olivine-hosted melt inclusions in the Dali picrites, Emeishan Large Igneous Province (LIP), SW China. These are the first *in-situ* Pb isotope data measured for melt inclusions found in the Emeishan picrites and allow new constraints to be placed on the source lithology of the Emeishan LIP. The melt inclusions show chemical compositional variations, spanning low-, intermediate- and high-Ti compositions, while their host whole rocks are restricted to the intermediate-Ti compositions. Together with the relatively constant Pb isotope ratios of the melt inclusions, the compositional variations suggest that the low-, intermediate- and high-Ti melts were derived from compositionally similar sources. The geochemical characteristics of melt inclusions, their host olivines, and whole-rocks from the Emeishan LIP indicate that Ca, Al, Mn, Yb, and Lu behave compatibly, and Ti, Rb, Sr, Zr, and Nb behave incompatibly during partial melting, requiring a pyroxenite source for the Emeishin LIP. The wide range of Ti contents in the melt inclusions and whole-rocks of the Emeishan basalts reflects different degrees of partial melting in the pyroxenite source at different depths in the melting column. The Pb isotope compositions of the melt inclusions and the OIB-like trace element compositions of the Emeishan basalts imply that mixing of a recycled ancient oceanic crust (EM1-like) component with a peridotite component from the lower mantle (FOZO-like component) could have underwent solid-state reaction, producing a secondary pyroxenite source that was subsequently partially melted to form the basalts. This new model of pyroxenite melting could explain the geochemical variations among the low-, intermediate- and high-Ti basalts for the Emeishan LIP and challenges the prevailing belief that the source of the Emeishan basalts is peridotite.

1. INTRODUCTION

Large igneous provinces (LIPs) are produced by some of the largest known volcanic episodes on our planet. Most

* Corresponding author at: State Key Laboratory of Isotope Geochemistry, Guangzhou Institute of Geochemistry, Chinese Academy of Sciences, 510640 Wushan, Guangzhou, China.
E-mail address: zyren@gig.ac.cn (Z.-Y. Ren).

http://dx.doi.org/10.1016/j.gca.2017.01.054
0016-7037/

LIPs contain relatively evolved tholeiitic basalts, typically having MgO contents <8 wt.%, and are either aphyric or only slightly porphyritic with little phenocrysts (Philpotts and Ague, 2009). However, geochemical mass balance calculations indicate that olivine, plagioclase and augite are primary phases of continental flood basalts (Philpotts and Ague, 2009). If multiple saturation is due to minerals fractionating at shallow depths, then what the primary magma was, where the fractionation took place, and what the lithology of the mantle source that can repeatedly supply enormous volumes of magma need to be constrained. However, these parameters are still not well known and a subject of debate.

The Emeishan LIP in SW China is one of the most significant LIPs in the world as it comprises several world-class giant V-Ti magnetite deposits and possesses some Cu-Ni-(PGE) sulphide deposits (Fig. 1; Zhou et al., 2005, 2008; Song et al., 2008a; Wang et al., 2008; Zhang et al., 2009). In addition, the Emeishan LIP is thought to be one of the best examples of a LIP generated by a mantle plume (e.g. Chung and Jahn, 1995; He et al., 2003; Xu et al., 2004; Ali et al., 2010). Furthermore, the Emeishan volcanism might have caused the end-Guadalupian mass extinction (Stanley and Yang, 1994; He et al., 2007; Ali et al., 2005; Wignall et al., 2009; Zhang et al., 2013; Zhong et al., 2014). In the last few decades, numerous petrological, geochemical, paleontological, paleomagnetic, geophysical, geochronological, and mineral deposit studies have been conducted on the Emeishan LIP.

Despite the breadth of understanding, there are still many controversies concerning the compositions of the primary magmas, the lithology of their sources, and the melting processes in the sources. It has long been believed that the source of the Emeishan basalts is peridotite, either from a mantle plume or the sub-continental lithosphere (e.g. Xu et al., 2001, 2007a; Xiao et al., 2004; Zhang et al., 2006; Hanski et al., 2010; Ali et al., 2010). Kamenetsky et al. (2012) suggested that the sources for the high-Ti and low-Ti lavas are garnet pyroxenite and peridotite in the sub-continental lithosphere mantle. Hou et al. (2013) interpreted that the Emeishan basalts originated from melts derived from the Emeishan mantle plume and from eclogite or pyroxenite in the lithospheric mantle.

Most of the previous petrological and geochemical studies on the Emeishan basalts are based on whole-rock compositions. Yet, whole-rocks are the final products resulting from complex petrogenesis involving partial melting in the mantle source, mixing of melts with different compositions in the magmatic plumbing system, assimilation of crustal materials in shallow magma chamber(s), and low temperature alteration. As a result specific source and primary magma composition information are retained in only a highly attenuated form or have completely disappeared from the bulk-rock compositions (Sobolev, 1996; Sobolev et al., 2000; Norman et al., 2002; Sun et al., 2003; Ren et al., 2005; Kent, 2008; Paul et al., 2011; Kamenetsky et al., 2012; Hong et al., 2013; Zhang et al., 2013; Liu et al., 2015; Qian et al., 2015). In contrast, melt inclusions 'frozen' in early crystallising high-Fo olivine phenocrysts can provide a detailed record of the primary magma compositions and their evolution in mafic lavas that may not always be available in whole-rock compositions (Sobolev, 1996; Sobolev et al., 2000; Danyushevsky et al., 2000; Norman et al., 2002; Sun et al., 2003; Ren et al., 2005; Kent, 2008; Hanski et al., 2010; Paul et al., 2011; Kamenetsky et al., 2012). In this paper, we present the first *in-situ* analysis of Pb isotopic ratios in olivine-hosted melt inclusions, from the Emeishan LIP, selected from the Dali picrites. These new data and the chemical compositions of the melt inclusions and their host olivines are combined with previously published melt inclusions from other picrites within the Emeishan LIP and whole-rock data, to better characterise the low-Ti and high-Ti lavas, estimate the primary magma compositions of the high-Ti and low-Ti type magmas, and explore their source lithology and melting processes.

2. GEOLOGICAL BACKGROUND

The Emeishan flood basalts, widely regarded as a LIP, cover >250,000 km^2 of southwestern China, forming a rhombic-shape province that includes parts of the Yunnan, Sichuan and Guizhou provinces on the western margin of the Yangtze craton (Fig. 1), and have a total volume of $>3 \times 10^5$ km^3 (Coffin and Eldholm, 1994; Chung and Jahn, 1995; Mahoney and Coffin, 1997; Chung et al., 1998; Xu et al., 2001, 2004; Ali et al., 2005; Xu et al., 2007b). They lie unconformably on limestones of the Early Late Permian Maokou Formation and are overlain unconformably in the east and west by sediments belonging to the uppermost Permian and in the central part by upper Triassic or Jurassic sediments (He et al., 2003). Liu and Zhu (2009) summarised the radiometric ages of the Emeishan LIP showing that the main phase of magmatism occurred over a short period of time, from 263 to 260 Ma, peaking at ~260 Ma. The thickness of the lavas varies from over 5000 m in the west (Yunnan province) to several hundred metres in the east (Guizhou province) (Chung et al., 1998; Xu et al., 2001; Ali et al., 2005). More than 95% of the volume of the Emeishan LIP is tholeiitic basalts with 4–8 wt.% MgO. Some picrites occur at various stratigraphic levels, and mafic alkaline lavas occur at the base and trachytes or rhyolites occur at the top of the sequence (Chung and Jahn, 1995; Xiao et al., 2004; Song et al., 2008a). Intrusive rocks include mafic and ultramafic dikes (Shellnutt et al., 2008; Zi et al., 2008) and larger layered intrusions, some of which host magmatic Ni-Cu sulphide and huge Fe-Ti-V oxide ore deposits (Zhou et al., 2005, 2008; Song et al., 2008a; Wang et al., 2008).

The Permian carbonates, which contain a record of the Guadalupian mass extinction, provide a potential link between the mass extinction and the Emeishan volcanism (Lo et al., 2002; Wignall et al., 2009; Zhang et al., 2013). Zhang et al. (2013) firstly studied S contents in melt inclusions from the Emeishan picrites and proposed a scenario in which large amounts of S were rapidly released into the atmosphere by Emeishan volcanism. This may have absorbed and reflected solar radiation, causing temperatures to drop, eventually leading to a 'volcanic winter' and the end-Guadalupian mass extinction.

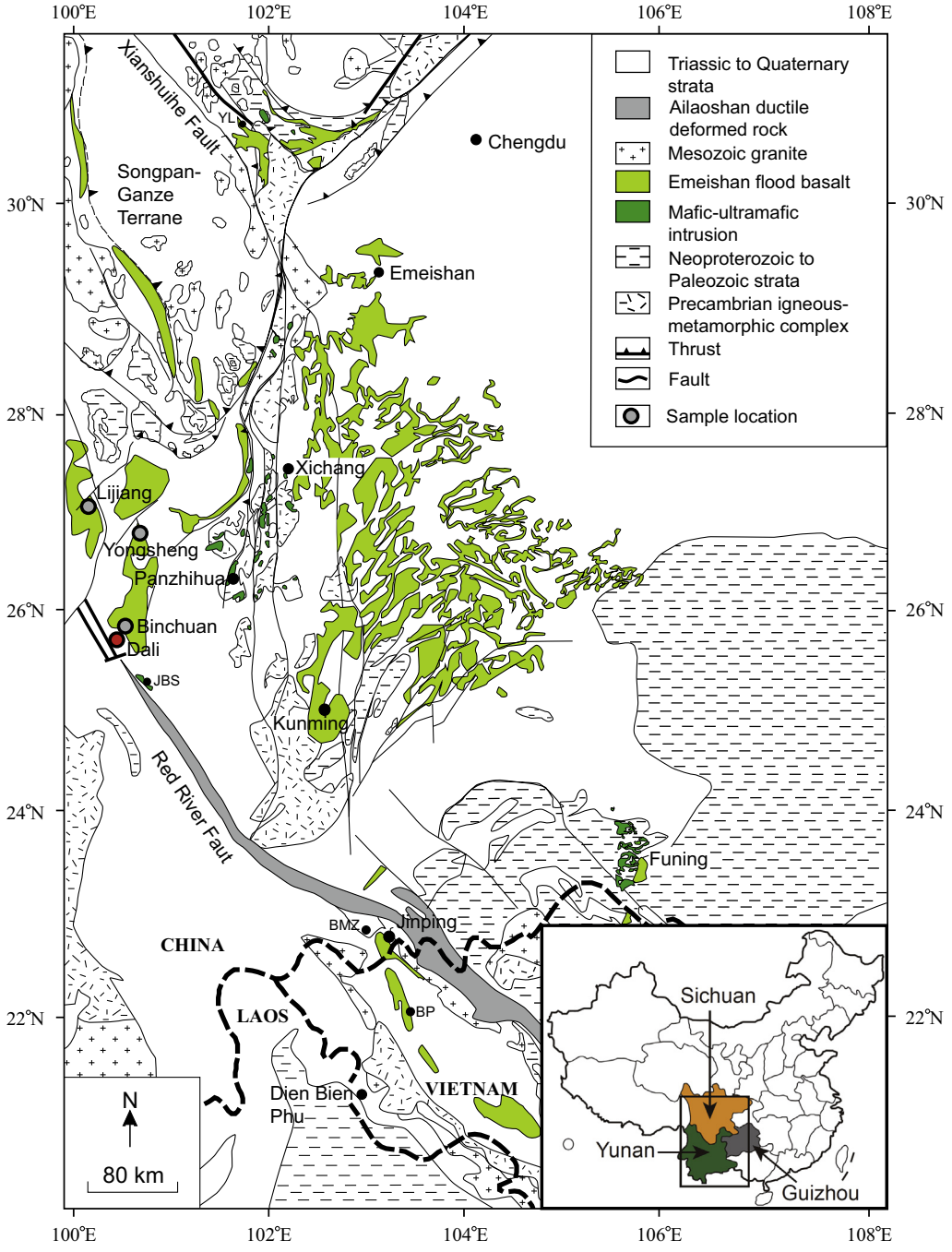

Fig. 1. The Emeishan Large Igneous Province (LIP), showing the distribution of volcanic and intrusive rocks (after Kamenetsky et al., 2012). The location of the Dali picrites collected in this study is shown by the red circle. Other picrite sampling localities (Binchuan, Yongsheng, Lijiang; see Chung and Jahn, 1995; Xu et al., 2001; Kamenetsky et al., 2012) are shown by the grey circles.

3. SAMPLES AND ANALYSES

3.1. Picritic lava samples

The picritic lavas mainly occur in the western part of the Emeishan LIP and are found at Dali, Binchuan, Yongsheng, and Lijiang (Fig. 1). The Dali picrites collected in this study are from a road cut section ca. 20 km NE of Dali (25°40′23.9″N; 100°21′23″E), as reported by Hanski et al. (2010).

Xu et al. (2001) and Xiao et al. (2004) divided the Emeishan basalts into two main types, low-Ti and high-Ti, based on the Ti/Y ratios and TiO_2 contents. Recently, Kamenetsky et al. (2012) proposed low-Ti and high-Ti

end-members, with an intermediate-Ti series that occur widely across the Emeishan LIP and form a continuous spectrum between the two end-members. They propose that the Binchuan picrites (Ti/Y as low as 300) represent the low-Ti end-member and the Yongsheng picrites with the highest Ti/Y ratios (ca. 800) represent the high-Ti end-member. The Dali and Lijiang picrites have intermediate Ti/Y ratios (Dali: 360–395; Lijiang: 630–700).

The Dali picrites have MgO contents of 17–21.6 wt.% (Li et al., 2014) and are highly porphyritic (up to ~50 vol. % phenocrysts). Phenocrysts include forsteritic olivine and clinopyroxene. The olivine phenocrysts are generally euhedral to subhedral and rarely embayed or partly resorbed. Most olivines range from 0.7 to 1 mm in size, although some are larger than 3 mm. Partial serpentinization has occurred along cracks within the crystals and at olivine margins. Some of the olivine phenocrysts are completely replaced by serpentine, but many grains retain cores of unaltered olivine, many of which contain scattered melt and spinel inclusions. Most melt inclusions are spherical, ranging from a few microns to tens of microns in diameter. Melt inclusions contain glassy melt or microcrystalline melt ± bubble ± Cr-spinel crystal (Fig. S1). The vapour bubble could have been trapped with the inclusion ('syngenetic' vapour bubble) or formed upon cooling ('shrinkage bubble') (Hauri, 2002). Spinel inclusions in the olivines are equant, euhedral to rounded, opaque to dark red-brown in colour, and range from a few microns to tens of microns across. Cr-spinel is also present as isolated grains in the groundmass. The groundmass surrounding the phenocrysts consists principally of very fine-grained anhedral clinopyroxenes and dendritic plagioclase microlites.

In this study, we also consider previously published data for melt inclusions and host olivines from the Binchuan, Dali and Yongsheng picrites, which span the low-, intermediate- and high-Ti compositions (Kamenetsky et al., 2012; Zhang et al., 2013).

3.2. Olivine and melt inclusion analytical techniques

A total of 709 unaltered melt inclusion-bearing olivine phenocrysts were selected from 16 Dali picrite samples under a binocular microscope. To acquire high quality data during analyses (e.g. using electron probe micro-analysis (EPMA) and laser ablation multiple-collector inductively coupled plasma mass spectrometry (LA-MC-ICP-MS)) of the chemical and isotopic compositions, it is almost always preferable to analyse a homogeneous glass rather than a mixture of various crystalline phases (e.g. Danyushevsky et al., 2002; Norman et al., 2002; Kent, 2008). The melt inclusions were rehomogenized to glass by reheating and quenching in a 1 atm furnace (e.g. Sobolev, 1996; Danyushevsky et al., 2002; Hauri, 2002; Norman et al., 2002; Ren et al., 2005; Kent, 2008; Hong et al., 2013; Zhang et al., 2013, 2014; Liu et al., 2015, 2016; Qian et al., 2015). The oxygen fugacity was maintained at the quartz-fayalite-magnetite buffer using a CO_2:H_2 gas mixture in the furnace. A platinum packet containing olivine grains was lowered into the furnace tube over 10 min and then held at 1250 °C for a further 10 min during which the crystal-glass mixture melted. The platinum packet was then rapidly raised back (within one second) to the top of the furnace tube to achieve homogeneous glassy inclusions. The reheated olivine grains were mounted on epoxy resin disks and polished with silicon carbide and diamond powder until the melt inclusions were exposed. All sample preparation was performed at the State Key Laboratory of Isotope Geochemistry, Guangzhou Institute of Geochemistry, Chinese Academy of Sciences (GIGCAS). The preparation procedures of melt inclusions were described in Ren et al. (2005).

The chemical compositions of the melt inclusions and olivines were analysed by EPMA using a JEOL JXA-8100 instrument at GIGCAS. To obtain precise data, we followed the procedures described in Sobolev et al. (2007) to analyse the melt inclusions. The accelerating voltage was 15 kV with a probe current of 2.0×10^{-8} A and a spot size of 3 μm. The melt inclusions were analysed for Na, K, Si, Al, Fe, Mg, Ca, Ti, Mn, and Ni. Because of the volatility of Na, it was analysed first and fast to minimise its possible loss during analysis. The analytical conditions of the EPMA for the melt inclusions are given in Table 1. Olivine analysis followed the procedures of Wang and Gaetani (2008) using an accelerating voltage of 20 kV, a probe current of 3.0×10^{-7} A and a spot size of 3 μm. Olivines were analysed for Si, Fe, Mg, Ca, and Ni. The analytical conditions of the EPMA of olivine are given in Table 1. In addition, to monitor instrumental drift, an internal glass standard (JB-2, Ren et al., 2004, 2005) and an olivine (from mantle peridotite xenolith, Hannuoba, Liu et al., 2015) were analysed before and after each batch of analyses. The external standard deviations (2σ) for each element in the monitoring standards are given in Table 1. One to three points were analysed in each melt inclusion and olivine and an average composition was calculated.

In-situ Pb isotope analysis of the melt inclusions was performed using a Neptune plus MC-ICP-MS and RESOlution M-50 laser ablation system. Zhang et al. (2014) have developed an analytical protocol for *in-situ* measurements of Pb isotopes in geological samples for spot size greater than 40 μm. The method is applicable to the analysis of Pb isotopes in melt inclusions which age correction for U-Th isotopic decay is required. We used spot sizes of 45 μm, an energy of 80 mJ, attenuation value of 25%, repetition rate of 3 Hz, and an integration time of 0.262 s enabling ablation time to be lengthened for data acquisition. In addition, to enhance the signal intensities of the Pb isotopes, Zhang et al. (2014) adopted a large dry interface pump (100 m^3 h^{-1} pumping speed), a Jet sample cone and a X skimmer cone, and added nitrogen gas with a flow rate of 2 ml/min. Standard-sample bracketing was employed to correct for mass bias and instrumental drift. The analysis routine employed eight ion counters to receive ^{238}U, ^{235}U, ^{232}Th, ^{208}Pb, ^{207}Pb, ^{206}Pb, ^{204}Pb and ^{202}Hg signals simultaneously, which allowed Hg interference to be corrected on ^{204}Pb, and, in old samples, U-Th decay to be age-corrected (see Zhang et al., 2014). The international basaltic glass standards NKT-1G and BHVO-2G that have similar ^{208}Pb intensities to the melt inclusions were selected to externally correct for mass bias, and evaluate the accu-

Table 1
The analytical conditions of electron probe microanalysis, and the analytical precisions of major oxides for olivine and melt inclusion.

Elements	Cryst	Line	Peak	BG (+)	BG (−)	Oxides	Analytical precision (wt%) (±2SD)
Olivine							Olivine[1]
Si	TAP	Kα	90	90	0	SiO_2	41.71 ± 0.17
Fe	LIF	Kα	90	90	0	FeO	9.43 ± 0.27
Mg	TAP	Kα	90	45	45	MgO	48.33 ± 0.29
Ca	PETH	Kα	120	60	60	CaO	0.043 ± 0.003
Ni	LIF	Kα	150	70	70	NiO	0.36 ± 0.034
Melt inclusion							JB-2 glass[2]
Si	TAP	Kα	20	20	20	SiO_2	53.57 ± 0.105
Ti	LIF	Kα	90	60	60	TiO_2	1.20 ± 0.006
Al	TAP	Kα	20	20	20	Al_2O_3	14.78 ± 0.062
Fe	LIF	Kα	20	20	20	FeO	13.01 ± 0.122
Mn	LIF	Kα	180	100	100	MnO	0.22 ± 0.042
Mg	TAP	Kα	20	20	20	MgO	4.68 ± 0.039
Ca	PETH	Kα	20	20	20	CaO	9.97 ± 0.041
Na	TAP	Kα	10	5	5	Na_2O	2.05 ± 0.026
K	PETH	Kα	10	5	5	K_2O	0.42 ± 0.011
P	PETH	Kα	60	40	40	P_2O_5	0.10 ± 0.023
Ni	LIF	Kα	180	100	100	NiO	0.01 ± 0.013

Notes: Acceleration voltage for olivine and melt inclusion of 20 kV and 15 kV, and probe current for olivine and melt inclusion of 3.0×10^{-7} A and 2.0×10^{-8} A, respectively. Peak and background (BG) counting time in seconds. BG (+) and BG (−) are the back ground of before and after element analysis, respectively. The analytical precisions for olivine and JB-2 glass monitor standard are given by mean ± standard deviation (2σ, $n = 140$ for olivine and $n = 160$ for JB-2 glass). Olivine[1] is from the Hannuoba mantle peridotite in China. JB-2 glass[2] is the Japanese basalt standard.

racy of the instrument prior to analysis. Before and after a batch of five melt inclusion analyses, the internal standard (BHVO-2G) was measured to monitor instrument drift. The Pb content of the BHVO-2G glass is 1.7 ppm, similar to that of the Emeishan melt inclusions (Zhang et al., 2014). Because of the low relative abundance of ^{204}Pb and the isobaric interference from ^{204}Hg, we present $^{207}Pb/^{206}Pb$ and $^{208}Pb/^{206}Pb$ of the melt inclusions. The average $^{208}Pb/^{206}Pb$ and $^{207}Pb/^{206}Pb$ given by the internal standard (BHVO-2G) as an unknown sample during the analysis of the melt inclusions are 2.056 and 0.834, in good agreement with the values recommended by Weis et al. (2005) (2.0524 and 0.8345, respectively). The external precisions are better than 0.27% for $^{208}Pb/^{206}Pb$ and 0.30% for $^{207}Pb/^{206}Pb$ (2σ, $n = 116$), whereas the accuracies are better than 0.16% for $^{208}Pb/^{206}Pb$ and −0.10% for $^{207}Pb/^{206}Pb$. Zhang et al. (2014) presented the detailed procedure of Pb isotope analysis of melt inclusions and the errors on the elemental concentrations for international standards of NIST 614, NKT-1G, TB-1G, NKT-1G, BHVO-2G.

4. RESULTS

4.1. Olivine compositions

The olivines from the Dali picrites analysed in this study and Zhang et al. (2013) range from $Fo_{80.2}$ to $Fo_{93.2}$ (Fig. 2). The Ca contents of the Dali olivines are similar to those of olivines from the intermediate-Ti picrites and low-Ti picrites, and higher than those of olivines from the high-Ti picrites. The Ni contents of the Dali olivines overlap those of the low-, intermediate- and high-Ti olivines (Fig. 2). Olivine compositions are provided in Electronic Appendix 1.

4.2. Melt inclusions

4.2.1. Chemical compositions

Melt inclusion compositions may be changed by crystallization and/or equilibration after entrapment (Danyushevsky et al., 2000, 2002; Kent, 2008). These changes are caused by crystallization of the host mineral on the inclusion walls or the crystallization of other daughter phases, and such processes have been experimentally reversed by remelting and homogenizing melt inclusions. In addition, olivine-hosted melt inclusions can re-equilibrate with their host olivine (Danyushevsky et al., 2000). This re-equilibration process, called "Fe-loss" mostly results in significantly higher MgO and lower FeO^T contents within the olivine-hosted melt inclusions (Danyushevsky et al., 2000), and cannot be reversed experimentally. The compositions of the olivine-hosted Emeishan melt inclusions have been corrected to account for Fe-loss, applying the widely accepted method of Danyushevsky et al. (2000), and were recalculated to be in equilibrium with the host olivine following the model of Ford et al. (1983) with the PETROLOG software (Danyushevsky and Plechov, 2011). This calculation requires an independent estimate of the initial trapped melt FeO^T content, which in most cases can be estimated from the FeO^T fractionation trend of the whole-rock samples (Danyushevsky et al., 2000, 2002). According to the FeO^T fractionation trend of the Dali picrite whole-rocks, 10.8 wt.% was set as the FeO^T content in the initial trapped

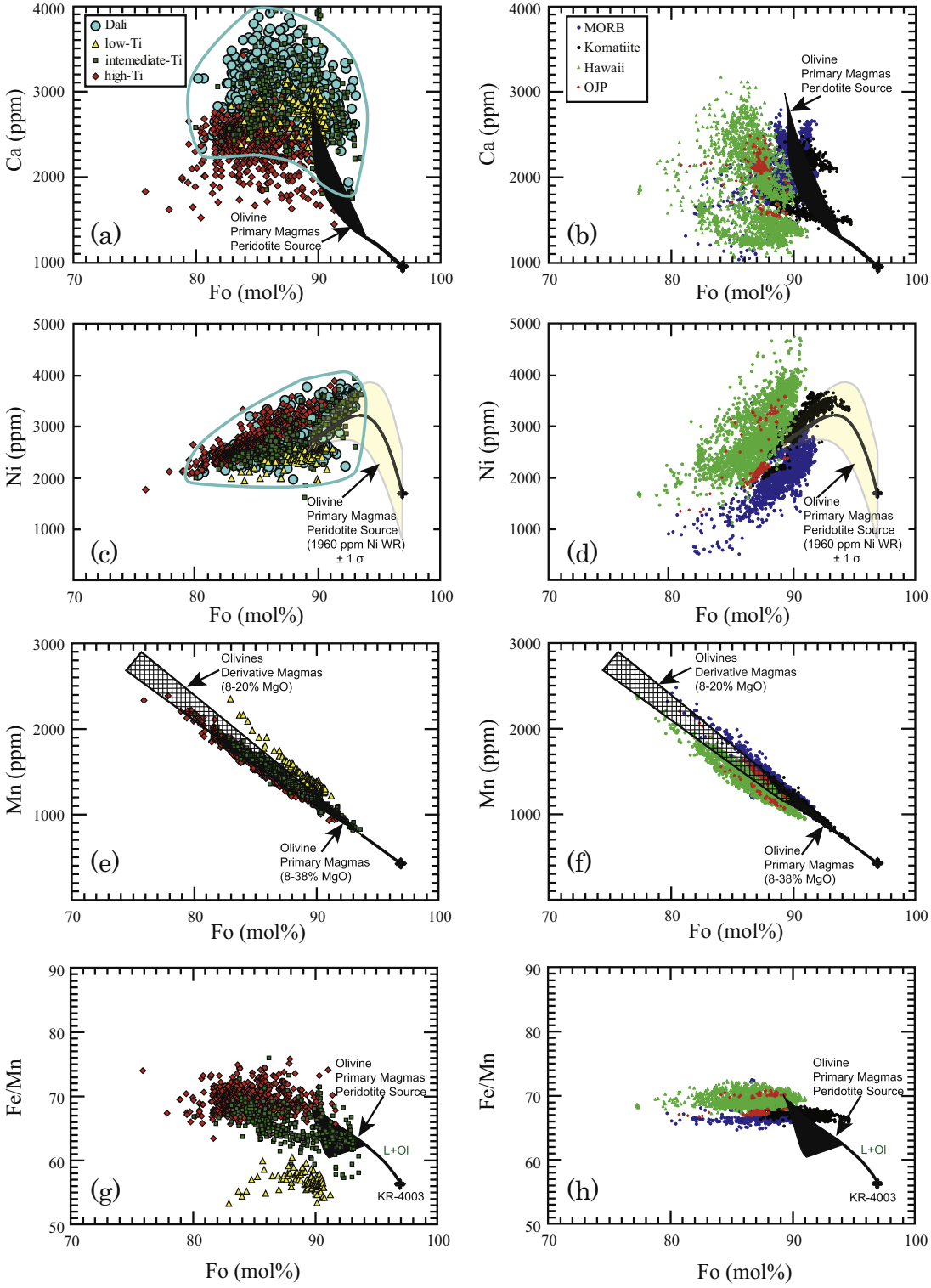

Fig. 2. (a) Ca, (c) Ni, (e) Mn and (g) Fe/Mn vs Fo calculated for olivine phenocrysts crystallised from partial melts of a peridotite source (Herzberg, 2011) compared to measured concentrations in olivines from the Emeishan picrites. Data for the Dali olivines are from this study and Zhang et al. (2013), intermediate-Ti olivines from Hanski et al. (2010) and Kamenetsky et al. (2012); low-Ti and high-Ti olivines from Kamenetsky et al. (2012). The olivine data of low-Ti from the Emeishan low- and high-Ti picrites reported in Kamenetsky et al. (2012) were also published in Sobolev et al. (2007) without being divided into low-, intermediate- and high-Ti types. (b) Ca, (d) Ni, (f) Mn and (h) Fe/Mn vs Fo for olivine phenocrysts from N-MORB, komatiite, Hawaiian shield, and Ontong Java Plateau (OJP) tholeiitic basalts, are shown for comparison. All the olivine data in these locations are from Sobolev et al. (2007).

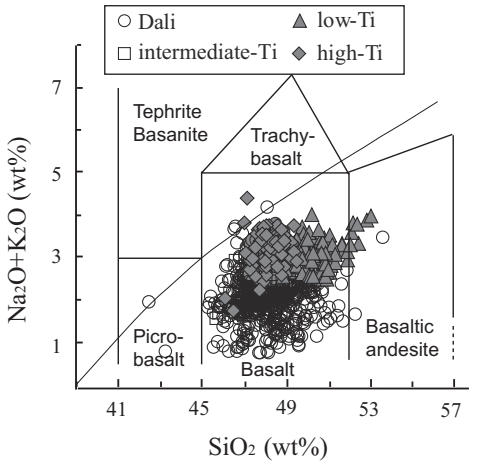

Fig. 3. $Na_2O + K_2O$ vs SiO_2 (wt.%) classification diagram showing that the Emeishan melt inclusions are tholeiitic basalts; only a few melt inclusions fall in the basaltic andesite, alkalic basalt, picrobasalt or alkalic picrobasalt fields. Data for the Dali melt inclusions are from this study and Zhang et al. (2013), intermediate-Ti melt inclusions from Hanski et al. (2010), and high-Ti and low-Ti melt inclusions from Kamenetsky et al. (2012). Compositional fields are from Le Bas et al. (1986).

melt (e.g. Zhang et al., 2013). The corrected melt compositions are listed in Electronic Appendix 2.

Almost all of the melt inclusions from the Dali picrites analysed in this study and by Zhang et al. (2013) are tholeiitic, with a corrected compositional range from 6.7 to 21.2 wt.% MgO and from 42.5 to 53.6 wt.% SiO_2. Only a few melt inclusions are basaltic-andesitic, alkali-basaltic, picrobasaltic or alkalic-picrobasaltic (Fig. 3). In melt inclusions with MgO $>\sim$ 10 wt.%, CaO and other oxides increase with decreasing MgO (Fig. 4), indicating fractionation of olivine. Between 10 and 7 wt.% MgO, CaO decreases and Al_2O_3 increases with decreasing MgO, which indicate that clinopyroxene starts fractionating without plagioclase. To avoid the effect of mineral fractionation other than olivine, we only use inclusions with MgO > 10 wt.%. At MgO > 10 wt.%, the TiO_2 contents of the Dali melt inclusions are similar to the intermediate-Ti melt inclusions. Some of the Dali melt inclusions overlap the fields of low-Ti or high-Ti melt inclusions (Fig. 4). The Al_2O_3 contents in the Dali melt inclusions are higher than those high-Ti melt inclusions and cover the fields of intermediate- and low-Ti melt inclusions. The melt inclusions also have a wide range of CaO contents at a given MgO content, overlapping the fields of low-Ti and high-Ti melt inclusions. The TiO_2/Al_2O_3 ratios of the Dali melt inclusions show a large variation, spanning the low-, intermediate- and high-Ti compositions (Fig. 5b). In spite of large variations in the Dali melt inclusions, the averaged melt inclusion compositions (e.g. TiO_2/Al_2O_3) are close to those of whole rocks (Fig. 5a). There is a good correlation between Ti/Y and TiO_2/Al_2O_3 ratios in the melt inclusions and whole rocks from the Emeishan picrites (Fig. 5b). Thus we could use TiO_2/Al_2O_3 ratio to characterise the low-, intermediate- and high-Ti lavas for the Emeishan LIP. Kamenetsky et al. (2012) also found that there are good correlations between Ti/Y with other trace element ratios (such as (Gd/Yb)n, Fig. 3 of Kamenetsky et al., 2012). Therefore, TiO_2/Al_2O_3 ratio is a favourable parameter to reflect the trace element characteristics of the Emeishan lavas.

4.2.2. Pb isotopes

The lead isotope data of 240 olivine-hosted melt inclusions from 12 Dali picrites are listed in Electronic Appendix 3 and are shown in Fig. 6. The measured $^{238}U/^{206}Pb$ and $^{232}Th/^{206}Pb$ are 0.1927–1.3334 and 0.8334–5.0304, respectively. The $^{208}Pb/^{206}Pb$ values vary from 2.028 to 2.101 with a mean value and a standard deviation (SD) of 2.067 and 0.014, respectively; the $^{207}Pb/^{206}Pb$ vary from 0.807 to 0.843, with a mean value and a standard deviation of 0.821 and 0.007, respectively (Fig. 6a). After U-Th correction (260 Ma), the $^{208}Pb/^{206}Pb$ and $^{207}Pb/^{206}Pb$ of the Dali melt inclusions have a narrower range from 2.061–2.118 and 0.833–0.862 with mean values of 2.091 (±0.010, 1SD) and 0.844 (±0.005, 1SD), respectively (Fig. 6a). The age-corrected Pb isotope ratios of the Dali melt inclusions plot in the field defined by the Emeishan tholeiitic whole-rock samples, but they show limited variation compared to the whole-rocks. The Pb isotopic compositions of the Dali melt inclusions fall within the field defined by the Ontong Java Plateau (OJP) tholeiitic basalts but with less variation. The Pb isotope compositions of the Dali melt inclusions are different from the Wrangellia high- and low-Ti basalts (Fig. 6b). The Wrangellia LIP, once existed as an oceanic plateau, has accreted to the western North American (Jones et al., 1977). The Pb isotope data of the Dali melt inclusions define an elongated array that extends between EM1 and FOZO components, with a few plotting in the Pacific MORB field. $^{208}Pb/^{206}Pb$ and $^{207}Pb/^{206}Pb$ of the Dali melt inclusions are relatively constant and show no correlation with Fo contents of the host olivine phenocrysts (Fig. 7a and b). The Pb isotope ratios also do not correlate with TiO_2 contents (Fig. 7e and f) or TiO_2/Al_2O_3 (Fig. 7g and h), despite TiO_2 and TiO_2/Al_2O_3 of the Dali melt inclusions spanning the entire range exhibited by the low-TiO_2 and high-TiO_2 Emeishan picrites. Even though there is a large variation of the MgO and SiO_2 in the melt inclusions, we suggest that crustal contamination plays a minor role and the Pb isotope compositions in the melt inclusions are primary (Fig. 7c and d). This new finding is consistent with the observation that the low-Ti and high-Ti Emeishan picrites are similar to each other in Sr-Nd isotope compositions (Kamenetsky et al., 2012). This implies that the low-, intermediate- and high-Ti magmas were derived from compositionally similar sources.

5. DISCUSSION

5.1. Genetic relationship between the olivine-hosted melt inclusions and the Dali picrites

The olivine-hosted melt inclusions from the Dali picrites show a large compositional diversity ranging from low-, intermediate- and high-Ti compositions (Figs. 4 and 5). The origin of the Dali melt inclusions and their host olivines

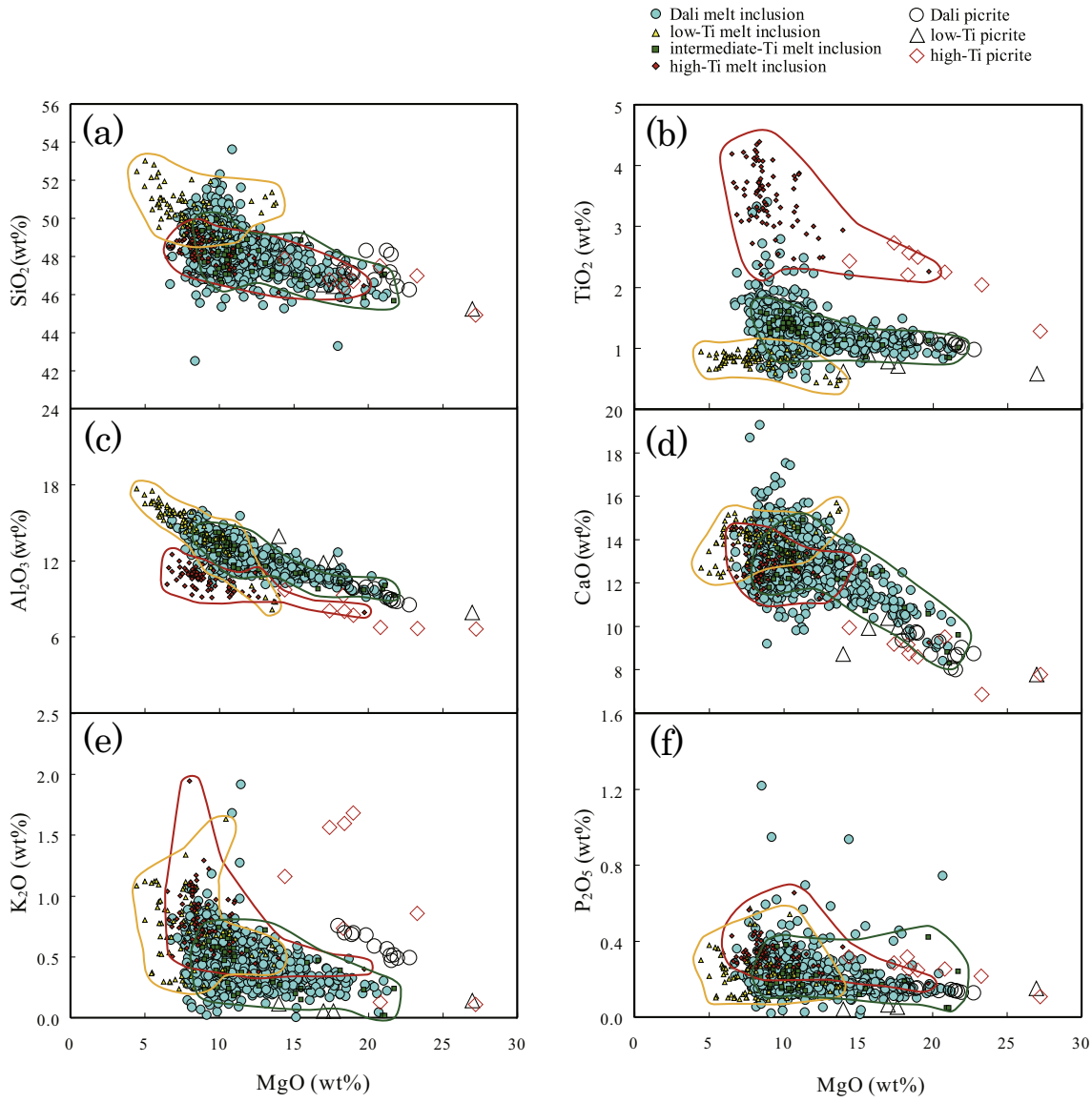

Fig. 4. MgO variation diagrams for the Emeishan melt inclusions. The data for the fields for the intermediate-Ti type are from Hanski et al. (2010) and Kamenetsky et al. (2012); the low-Ti and high-Ti types are from Kamenetsky et al. (2012). The whole-rock data for the Dali picrites are from Li et al. (2010); those for the low-Ti and high-Ti picrites are from Kamenetsky et al. (2012).

should be understood before further discussion on the petrogenesis of the Emeishan basalts. We believe that the Dali melt inclusions and their host olivine phenocrysts are genetically related to the Dali picrites. The reasons are as follows: (1) The well-preserved primary melt inclusions randomly distributed in olivines (Fig. S1) from the Dali picrites indicates that the studied olivines all crystallized from a magma rather than being mantle-derived xenocrysts. (2) Typical poikilitic texture, in which large clinopyroxenes envelop euhedral olivines, can be observed in the thin sections from the Dali picrites. In addition, we observed that fresh olivines are generally euhedral to subhedral and contain Cr-spinel inclusions under microscope. These textures indicate magmatic genesis of these olivines. (3) The olivines in the Dali picrites have high CaO contents (>0.24 wt.%, Fig. 2), while CaO contents in olivines from the mantle peridotites (e.g. Thompson and Gibson, 2000; Ren et al., 2004; Putirka et al., 2007) and mafic-ultramafic accumulate intrusions (Charlier et al., 2011; Yudovskaya et al., 2013; Wang et al., 2014) are usually less than 0.2 wt.%. So the xenocrysts origin of these olivines could be excluded. (4) The compositions of the Dali melt inclusions define the same compositional trends with the whole rocks from the Emeishan picrites (Fig. 4). In addition, despite the large variation of TiO_2/Al_2O_3 ratios in the Dali melt inclusions, the averaged TiO_2/Al_2O_3 ratios closely correspond with those of the Dali whole rocks (Fig. 5a). The similarity between the averaged melt inclusion compositions and the whole-rock compositions is not the case in the Dali picrites and in the low-Ti and high-Ti picrites from the Emeishan

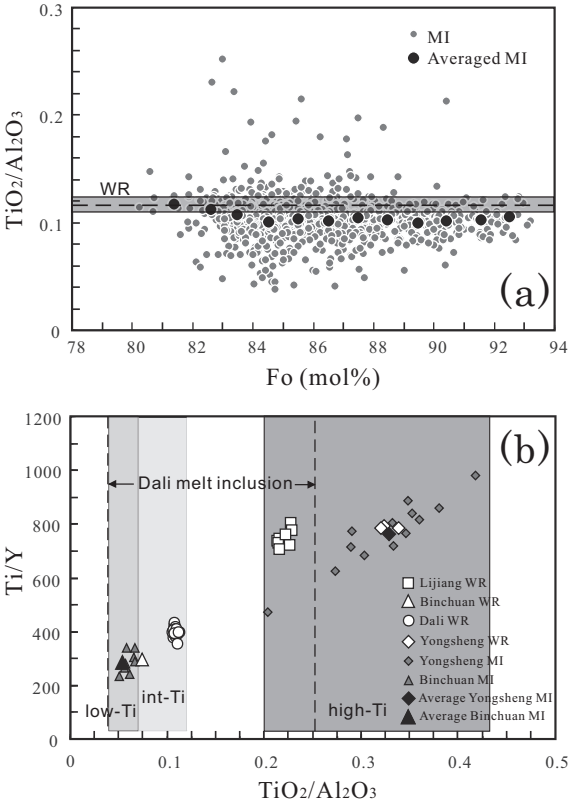

Fig. 5. (a) Variation diagram between TiO_2/Al_2O_3 ratios in the melt inclusions and Fo values of their host olivines from the Dali picrites. The black dots represent average TiO_2/Al_2O_3 ratios in the melt inclusions which are calculated at each Fo interval. The dashed line with "WR" mark and the shadow area are averaged and total range of TiO_2/Al_2O_3 ratios of the Dali whole rock. (b) Variation diagram between Ti/Y ratios and TiO_2/Al_2O_3 ratios of whole rocks, melt inclusions, and average melt inclusions. The average melt inclusion compositions are similar to those of whole rocks. There is a good correlation between Ti/Y and TiO_2/Al_2O_3 ratios for the melt inclusions and whole rocks from the Emeishan picrites, so the TiO_2/Al_2O_3 ratio could be used to characterise the low-, intermediate- and high-Ti Emeishan lavas. The Dali whole rock compositions are from Hanski et al. (2010) and Li et al. (2014); the Binchuan and Yongsheng whole rock and melt inclusion compositions are from Kamenetsky et al. (2012); the Lijiang whole rock compositions are from Hanski et al. (2010). Abbreviations: WR, whole rock; MI, melt inclusion; int-Ti, intermediate-Ti.

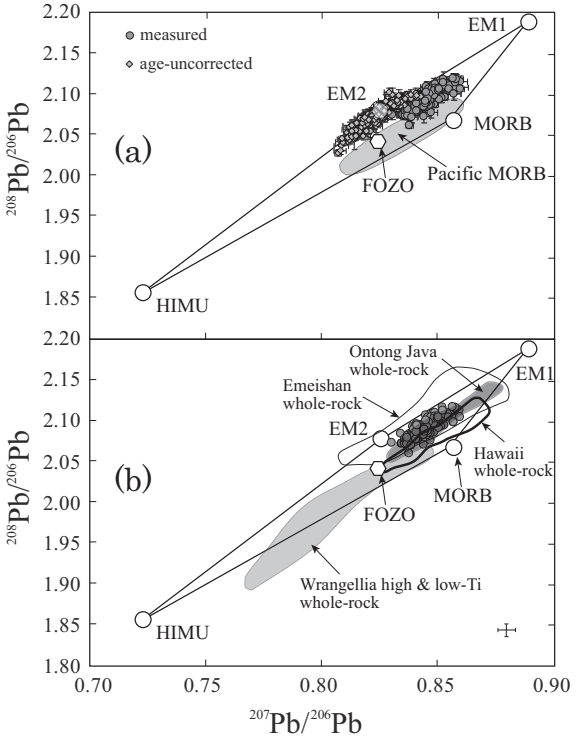

Fig. 6. The Pb isotope ratios for melt inclusions from the Dali picrites (a) melt inclusions with age-corrected Pb isotope ratios compared to those of measured data and Pacific MORB; (b) melt inclusions with age-corrected Pb isotope ratios compared to fields for whole-rock data of basalts from the Emeishan LIP, OJP, Hawaiian shield, and Wrangellia Plateau (high-, and low-Ti lavas), and mantle end-members. *Data sources*: Emeishan basalts are from Zhang et al. (2006, 2008), Xu et al. (2007a), Fan et al. (2008), Lai et al. (2012). OJP basalts are from Mahoney et al. (1993a, b), Tejada et al. (1996, 2002, 2004), Hawaiian shield basalts are from Pietruszka and Garcia (1999), Tanaka et al. (2002, 2008), Blichert-Toft et al. (2003), Eisele et al. (2003), Coombs et al. (2004), Kimura et al. (2006), Ren et al. (2006, 2009), Abouchami et al. (2005), Marske et al. (2007), Xu et al. (2005, 2007c), Wanless et al. (2006), Fekiacova et al. (2007), Yamasaki et al. (2009), Garcia et al. (2010), Weis et al. (2011). Wrangellia basalts are from Greene et al. (2008, 2009a, 2009b). The EM1, EM2, HIMU, MORB and FOZO end-members are from Saal et al. (1998, 2005). Field for Pacific MORB is from Paul et al. (2011). The results show that it is necessary to age-correct data for the Emeishan melt inclusions. The age-corrected (260 Ma) Pb isotope ratios of the Dali melt inclusions define a linear array between EM1 and FOZO components. The error bars for the Dali melt inclusions are shown (2σ).

LIP only, but seems to be a ubiquitous phenomenon found in mid-ocean ridge basalts (e.g. Sobolev, 1996; Kamenetsky et al., 1997; Sours-Page et al., 1999) and continental flood basalts (e.g. Kent et al., 2002; Slater et al., 2001; Maclennan, 2008). Numerous studies on olivine-hosted melt inclusions indicate that erupted lava compositions represent blended mixtures of a number of different melt compositions, whereas melt inclusions sample this diversity and protect trapped melts from subsequent mixing and blending (e.g. Sobolev and Shimizu, 1993; Nielsen et al., 1995, 2000; Sobolev, 1996; Kent et al., 1999, 2002; Slater et al., 2001; Norman et al., 2002; Maclennan, 2008; Ren et al., 2005; Paul et al., 2011; Hong et al., 2013; Liu et al., 2015; Qian et al., 2015). Melt inclusions can be considered as the unmixed (or less-mixed) equivalents of erupted lavas (Sobolev, 1996; Norman et al., 2002; Saal et al., 1998, 2005; Ren et al., 2005; Kent, 2008; Liu et al., 2015). (5) As suggested by Shellnutt et al. (2015), remelting of pre-existing mafic/ultramafic bodies in the lower crust might be a mechanism producing some Emeishan basalts. If the olivines containing melt inclusions of the Dali picrites have different origins (e.g. some of olivines in the Dali picrites might be derived from crystallizing in melts from remelting of pre-existing mafic/ultramafic bodies in the lower crust

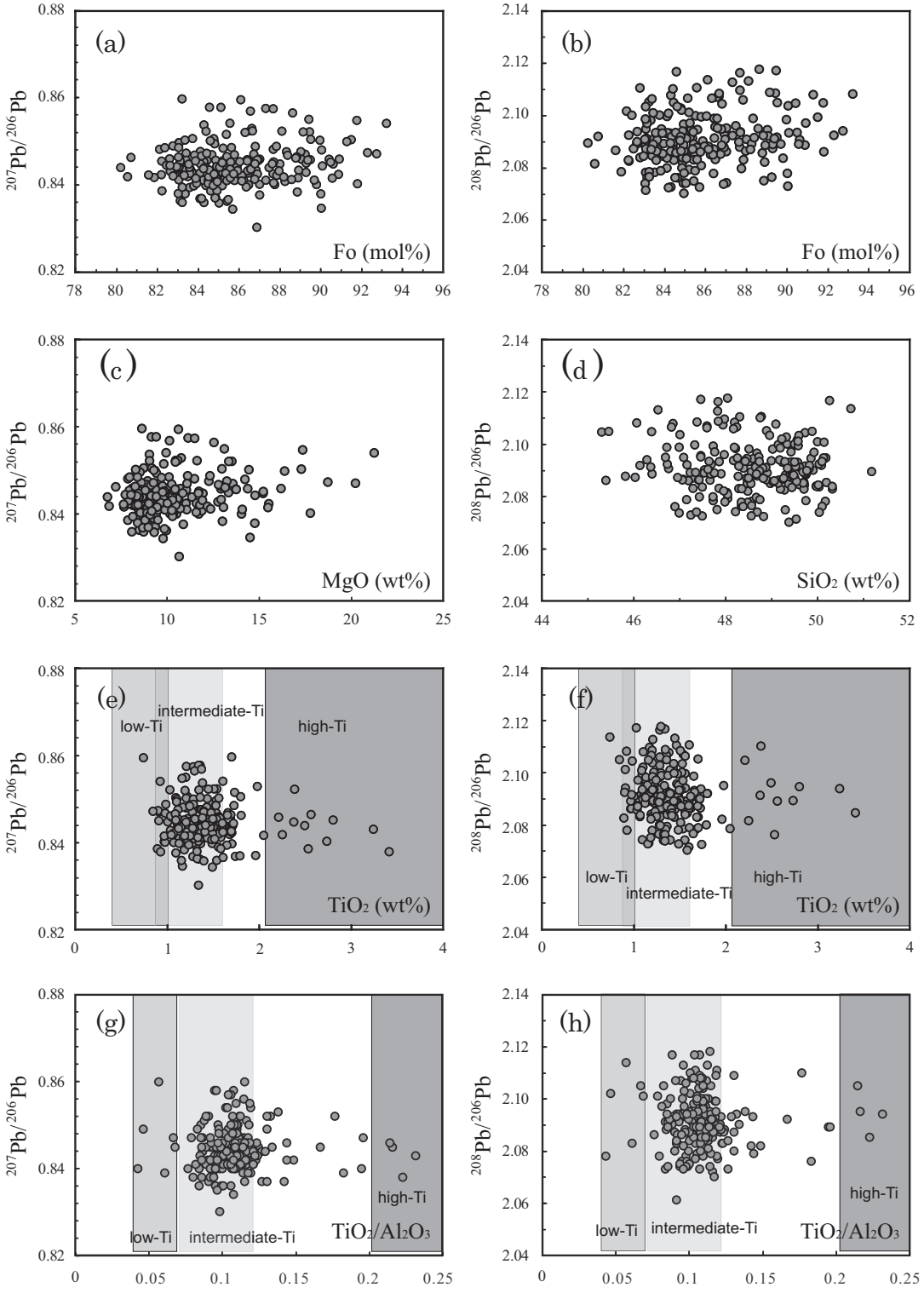

Fig. 7. (a) $^{207}Pb/^{206}Pb$ vs Fo, (b) $^{208}Pb/^{206}Pb$ vs Fo, (c) $^{207}Pb/^{206}Pb$ vs MgO, (d) $^{208}Pb/^{206}Pb$ vs SiO_2, (e) $^{207}Pb/^{206}Pb$ vs TiO_2, (f) $^{208}Pb/^{206}Pb$ vs TiO_2, (g) $^{207}Pb/^{206}Pb$ vs TiO_2/Al_2O_3, and (h) $^{208}Pb/^{206}Pb$ vs TiO_2/Al_2O_3 for the Dali melt inclusions. The Dali melt inclusions have a narrow range of $^{207}Pb/^{206}Pb$ and $^{208}Pb/^{206}Pb$ that do not correlate with Fo contents of host olivines, and the MgO and SiO_2 contents of the melt inclusions. The TiO_2 and TiO_2/Al_2O_3 ratios of the melt inclusions from the Dali picrites span the low-Ti, intermediate-Ti and high-Ti fields for Emeishan melt inclusions (data for the fields are from Kamenetsky et al., 2012), and do not correlate with the relatively small variations in $^{207}Pb/^{206}Pb$ and $^{208}Pb/^{206}Pb$ ratios.

and/or derived from capturing olivines from pre-existing ultramafic bodies), the Pb isotope compositions of the olivine-hosted melt inclusions are expected to be heterogeneous. However, the opposite phenomenon is observed. The Pb isotope compositions in the Dali melt inclusions show limited variation and are relatively homogenous (Fig. 6). Also, the Pb isotope compositions have no correlation with Fo contents of the host olivine phenocrysts and the MgO and SiO_2 contents in the melt inclusions (Fig. 7), implying that the melt inclusions are not derived from melts that were from remelting of pre-existing mafic/ultramafic bodies in the lower crust and/or derived from capturing olivines from pre-existing ultramafic bodies. Furthermore, almost all the Dali melt inclusions (>98%) have high MgO contents above 8 wt.%, that unrealistic high degrees of partial melting of the lower crust rocks are needed to form these high MgO magmas (see Fig. 6 of Shellnutt et al., 2015).

In summary, the Dali melt inclusions and their host olivine phenocrysts are genetically related to the Dali picrites. The Dali picrites can be explained to be the aggregation of a range of diverse melts sampled by the Dali melt inclusions approximately the same as its contribution to the host picrites. The Dali melt inclusions, which have a large compositional diversity spanning from low-, intermediate- and high-Ti compositions (Figs. 4 and 5), represent diverse unmixed or less mixed melts that aggregate and mix subsequently in deep magma chamber(s) or channels to produce the Dali picrites and that should also contribute to the whole Emeishan basalts. Thus, the Dali melt inclusion compositions can be used to constrain on the origin of the Emeishan basalts.

5.2. Primary magmas of low-, intermediate- and high-Ti lavas

There have been many estimates of the primary magma compositions of Emeishan picrites (Xu and Chung, 2001; Hanski et al., 2004; Zhang et al., 2006; Ali et al., 2010). Xu and Chung (2001) estimated that the primary magma compositions of the picrites range between 16 and 18 wt.% MgO. Using the highest Fo content of olivine (93.5 mol%) found in the Dali picrites, Hanski et al. (2010) suggested that the primary magmas of the Dali picrites had an MgO content of ~23 wt.%. On the basis of the highest Fo content of olivine (91.6 mol.%) from the picrites in the Lijiang area, Zhang et al. (2006) estimated their primary magma contain 22 wt.% MgO.

Most of these previous estimates of the primary magma were based on whole-rock compositions of mafic lavas in equilibrium with the composition of the highest Fo content of olivine found in the lavas. However, whole-rock compositions might be affected by magma mixing, contamination from wall rocks and post-magmatic alteration. Indeed, the Emeishan lavas have been extensively affected by low temperature alteration (e.g. Fig. 8). Also they have been extensively contaminated by felsic crust (Fig. 9).

Some of the estimates are based on the assumption that the primary magma is in equilibrium with peridotite in the source; if this assumption is invalid, and the source is something else, such as pyroxenite, the estimates are unreliable. The best estimates of primary magma composition come from early crystallising high-Fo olivine-hosted melt inclusions because they represent more primitive magma compositions prior to extensive magma mixing and provide a higher resolution of the magmatic processes than whole-rocks (e.g. Sobolev, 1996; Danyushevsky et al., 2000, 2002; Hauri, 2002; Norman et al., 2002; Sun et al., 2003; Ren et al., 2005; Kent, 2008; Kamenetsky et al., 2012; Zhang et al., 2013; Liu et al., 2015). In addition, using melt inclusions to estimate primary magmas may minimise the compositional effects caused by post-magmatic processes. Here, we used the compositions of the melt inclusions from the Dali picrites and from the other Emeishan picrites involving low-, intermediate- and high-Ti groups to estimate the primary magma compositions of the low-, intermediate- and high-Ti magmas. Only corrected melt inclusion data with MgO > 10 wt.% were used in the calculation. The selected major element data of the melt inclusions were adjusted to a constant Fe^{2+}/Fe_{total} ratio of 0.9 along the QFM buffer, and then olivine was added in 0.1 wt.% increments until the melt inclusion composition was in equilibrium with $Fo_{93.5}$, the most forsteritic olivine found in the Emeishan picrites (Hanski et al., 2010). The calculated primary magma compositions of the low-, intermediate- and high-Ti magma types (Electronic Appendix 3) show systematic compositional variations (Fig. 10). This variations indicate that melt inclusion compositions in equilibrium with a certain olivine composition ($Fo_{93.5}$) are not uniform in composition, implying that the primary magmas have a wide range of compositional variation. The calculation of the primary magmas using other Fo contents does not affect our subsequent conclusions, but it is useful to correct for the effects of olivine fractionation and to evaluate the compositional characteristics of different types of magmas (e.g. Hauri, 1996; Frey et al., 2000). The calculated results indicate that the low-, intermediate- and high-Ti primary magmas have MgO contents ranging from 14.5–18.1, 18.1–21.8, and 19.6–23.2 wt.%, respectively (Fig. 10, Electronic Appendix 3). The low-Ti primary magmas have higher SiO_2, Al_2O_3, CaO, MnO, and Na_2O contents and lower MgO contents than those of the high-Ti primary magmas (Fig. 10). The major element compositions of the intermediate-Ti primary magmas (including the Dali primary magma) are between those of the low- and high-Ti primary magmas.

Hou et al. (2011) reappraised the classification of the low-Ti and high-Ti Emeishan basalts and suggested that the differences between the low-Ti and high-Ti types are results from mineral fractionation. However, the compositional diversity between the low-, intermediate- and high-Ti primary magmas cannot be explained by mineral fractionation. Furthermore, for a given Fo content, olivine compositions from the high-Ti picrites are consistently lower in Mn and Ca and higher in Fe/Mn and Ni compared to those of olivines from the low-Ti picrites (Fig. 2). This also reflects that the different magma types, from which different types of olivine crystallized, evolved from different parental magmas.

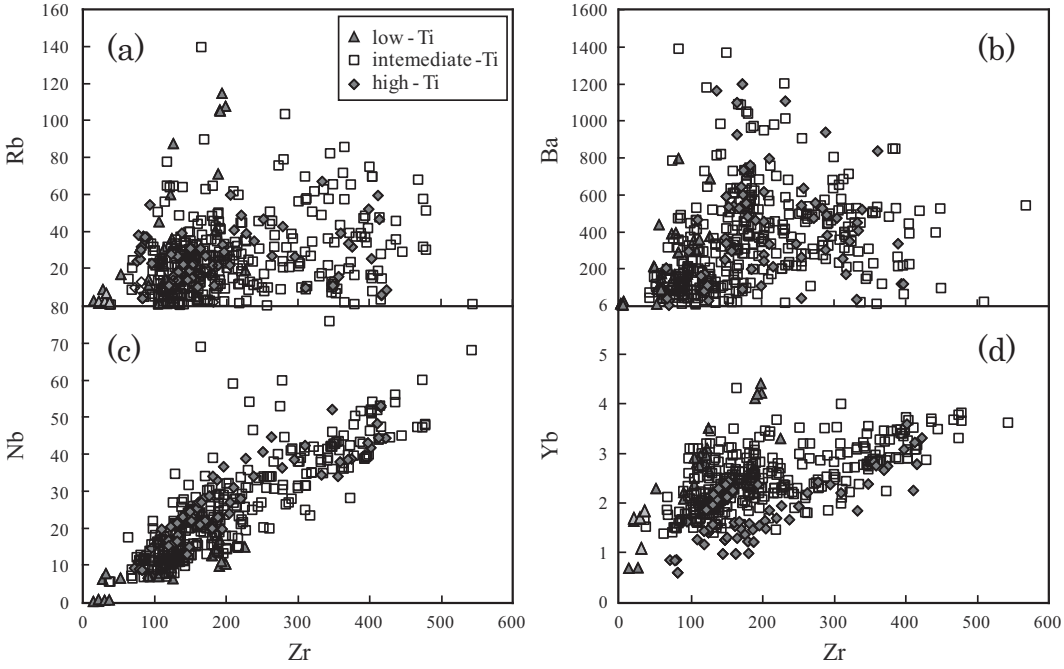

Fig. 8. Mobile (Rb, Ba) and immobile (Nb, Yb) trace element abundances versus Zr content (ppm) in Emeishan basaltic-picritic whole-rocks. The poor correlations between the mobile elements and the immobile element Zr, and relatively good correlations between the immobile elements reflect post-magmatic alteration of the Emeishan lavas. Data for the Emeishan lavas are from Xiao et al. (2003, 2004), Song et al. (2004, 2006, 2008b), Xu et al. (2001, 2007a), Zhang et al. (2006), Zhou et al. (2006), Wang et al. (2007), Qi et al. (2008), Fan et al. (2008), Li et al. (2010), and are available on the GEOROC Database (http://georoc.mpch-mainz.gwdg.de/georoc/).

5.3. Source mineralogy and lithology

It has long been advocated that peridotite was the source of the Emeishan basalts, occurring either in mantle plume or sub-continental lithosphere peridotite (Xu et al., 2001, 2004, 2007b; Xiao et al., 2004; Zhang et al., 2006; Hanski et al., 2010; Kamenetsky et al., 2012). Xu et al. (2001, 2004), on the basis of spatial distribution of the low-Ti and high-Ti basalts and their different age-corrected $^{87}Sr/^{86}Sr$ and $^{143}Nd/^{144}Nd$ ratios, proposed that the low-Ti magmas were derived from a higher degree of partial melting in the central part of a spinel-peridotite plume source at shallower depth, whereas the high-Ti magmas were derived from a lower degree of melting of the mantle peridotite source at the plume margin at greater depth. Xiao et al. (2004) indicated that the low-Ti type magmas are formed from the enriched sub-continental lithospheric mantle (SCLM), whereas the high-Ti magmas originated from a plume source at deeper depth. Xu et al. (2007a) analysed Os isotopic compositions in 21 Emeishan low-Ti and high-Ti basalts, and concluded that the low-Ti basalts with higher Os concentrations have a radiogenic Os isotopic compositions, similar to that of plume-derived OIB, whereas the high-Ti basalts with higher Os concentrations have unradiogenic Os isotopic signatures, suggesting a contribution from subcontinental lithospheric mantle to the source. Kamenetsky et al. (2012) suggested that peridotite and garnet pyroxenite in the sub-continental lithospheric mantle are responsible for the source of the low-Ti and high-Ti magmas, respectively. However, Zhang et al. (2006, 2008, 2009) analysed Nd, Pb, and Sr isotope ratios of mafic rocks from the Lijiang, Daju picrites and clinopyroxenes from the Panzhihua (high-Ti), Xinjie (high-Ti), Limahe (low-Ti) intrusions from the Emeishan LIP and concluded that there are no correlations between isotopic ratios and Ti/Y of the Emeishan mafic rocks.

Previously published isotopic data of the basalts from the Emeishan LIP (Fig. 12) show huge variations; the ranges of Sr, Nd, Pb isotopes are far greater than those of tholeiitic basalts from the Hawaiian shield, OJP and Wrangellia Plateau. There are no correlations between Ti/Y ratios and the Sr, Nd, and Pb isotope compositions of the Emeishan basalts (Fig. 12), consistent with the conclusion of Kamenetsky et al. (2012) (Fig. 11 of Kamenetsky et al., 2012). As stated above, the Emeishan basalts have been widely affected by low temperature alteration (e.g. Fig. 8) and contamination by felsic crust (Fig. 9). The Sr, Nd isotopic ratios of the Emeishan basalts show a trend towards the continental crust (Fig. 12), also indicating that they have been contaminated by continental crust. Considering the alteration and contamination effects, the age-corrected isotopes of the whole-rocks may not represent the real or primary mantle source isotopic compositions at the time of their eruption. *In-situ* Pb isotopic analyses in the unaltered olivine-hosted melt inclusions from the Dali picrites analysed in this study will be far more reliable. The Pb isotopic compositions of the Dali melt inclusions show no correlation with the Fo contents of the host olivine phenocrysts (Fig. 7a and b). Together with the large variations of the MgO and SiO_2 in the melt

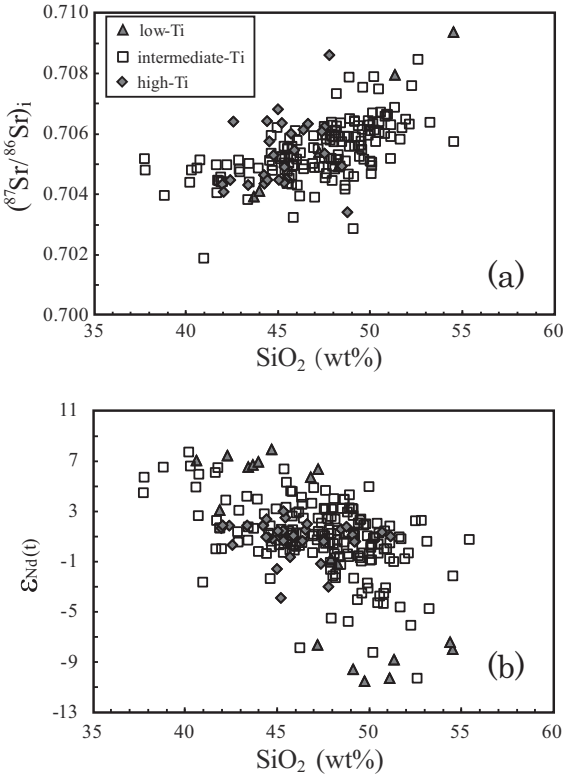

Fig. 9. Initial (260 Ma) $^{87}Sr/^{86}Sr$ and ε_{Nd} vs SiO_2 (wt.%) for picritic-basaltic whole-rocks from the Emeishan LIP. They show that as $^{87}Sr/^{86}Sr$ increases, ε_{Nd} decreases with increasing SiO_2, indicating that the Emeishan basalts are contaminated by felsic crustal melts. Emeishan whole rock data are from Chung and Jahn (1995), Xu et al. (2001, 2007a), Hanski et al. (2004, 2010), Xiao et al. (2004), Song et al. (2004, 2006, 2008b), Zhou et al. (2006), Zhang et al. (2006, 2008), Wang et al. (2007), Fan et al. (2008), Qi et al. (2008) and Li et al. (2010).

inclusions, these observations imply that the compositions of the melt inclusions are not affected by crustal contamination (Fig. 7c and d). Despite TiO_2 and TiO_2/Al_2O_3 of the Dali melt inclusions spanning from the low-, intermediate- to the high-Ti Emeishan melt inclusions (Figs. 4 and 7), the Pb isotopic ratios show an even narrower range than the OJP tholeiites. The OJP, world's largest oceanic plateau, has a narrow range of Nd-Sr-Pb-Hf (Mahoney, 1987; Mahoney et al., 1993a,b; Tejada et al., 1996, 2002, 2004, 2013), which is unique among LIPs, suggesting a relatively homogeneous mantle source (Tejada et al., 2004). The relatively constant Pb isotope compositions of the Dali melt inclusions, together with the similar isotope compositions from the low-Ti and high-Ti Emeishan picrites (Kamenetsky et al., 2012) and the very similar trace element patterns in the alteration-resistant clinopyroxene phenocrysts from the low-, intermediate- and high-Ti Emeishan picrites (Kamenetsky et al., 2012), imply that the compositional diversity of the low-, intermediate- and high-Ti lavas reflects various degrees of melting of a relatively homogeneous source rather than heterogeneous sources. The field defined by the $^{207}Pb/^{206}Pb$ and $^{208}Pb/^{206}$-Pb ratios of the Wrangellia Plateau is remarkably different from that defined by the Dali inclusions (Fig. 6), implying that the Wrangellia Plateau and Emeishan LIP have different sources.

The compositions of the primary magmas for the low-, intermediate- and high-Ti lavas (Fig. 10) can be used to evaluate the residual mineralogy of the source. The CaO content in the primary magmas slightly increases with decreasing TiO_2 content (Fig. 13a), implying residual clinopyroxene in the source. This is because TiO_2 is incompatible and it decreases with increasing degrees of melting of pyroxenite and peridotite (Walter, 1998; Kogiso et al., 1998, 2003, 2004), whereas CaO is buffered by residual clinopyroxene (e.g. Ren et al., 2004). CaO is more likely to behave compatibly during partial melting of a clinopyroxene-rich source (Yasuda et al., 1994; Kogiso et al., 1998), because Ca is compatible in clinopyroxene ($D_{Ca}^{Cpx} = 1.82–1.95$, Pertermann and Hirschmann, 2002). In contrast, CaO is extremely incompatible in peridotite (Walter, 1998) and thus should decrease dramatically in melts of peridotite with increasing degrees of melting, resulting in negative correlations between CaO and TiO_2. Nearly constant CaO/Al_2O_3 with decreasing TiO_2 content (Fig. 13d) implies that a clinopyroxene-rich source controls the Emeishan primary magma compositions. CaO/Al_2O_3 will decrease rapidly with increasing degree of melting of the peridotite (e.g. Walter, 1998).

The compositions of the primary magmas also suggest that garnet was a major residual phase. Al_2O_3 shows slightly negative correlation with TiO_2 in the primary magma compositions (Fig. 13b), which can be attributed to buffering of Al by residual garnet. TiO_2 decreases with increasing degrees of melting, whereas Al_2O_3 slightly increases because it is more likely to be compatible during partial melting of a garnet-rich source (e.g. Ren et al., 2004).

In summary, the primary magma compositions estimated from the melt inclusion compositions suggest that the source lithology for the Emeishan lavas is garnet-rich pyroxenite.

5.4. Melting processes in the source

As discussed above, the Emeishan lavas were derived from a relatively homogeneous pyroxenite source rather than heterogeneous sources. A number of experimental results indicate that pyroxenite could generate picritic melts (Kogiso et al., 1998, 2003; Takahashi and Nakajima, 2002; Sobolev et al., 2005; Tuff et al., 2005; Herzberg, 2006). The compositional variation of the low-, intermediate- and high-Ti primary magmas reflect the diversity in degrees of partial melting.

Titanium is incompatible during the partial melting of pyroxenite, and low degree partial melts will have higher Ti contents (Kogiso et al., 2003, 2004). In addition, the high Al_2O_3 and CaO contents in the low-Ti melt inclusions (Fig. 4c and e) also suggest that they were derived from high degrees of melting of a pyroxenite source, which can release Ca from garnet and clinopyroxene and Al from garnet, resulting in higher CaO and Al_2O_3 contents in the melts (Kogiso et al., 1998; Ren et al., 2004; Herzberg, 2011).

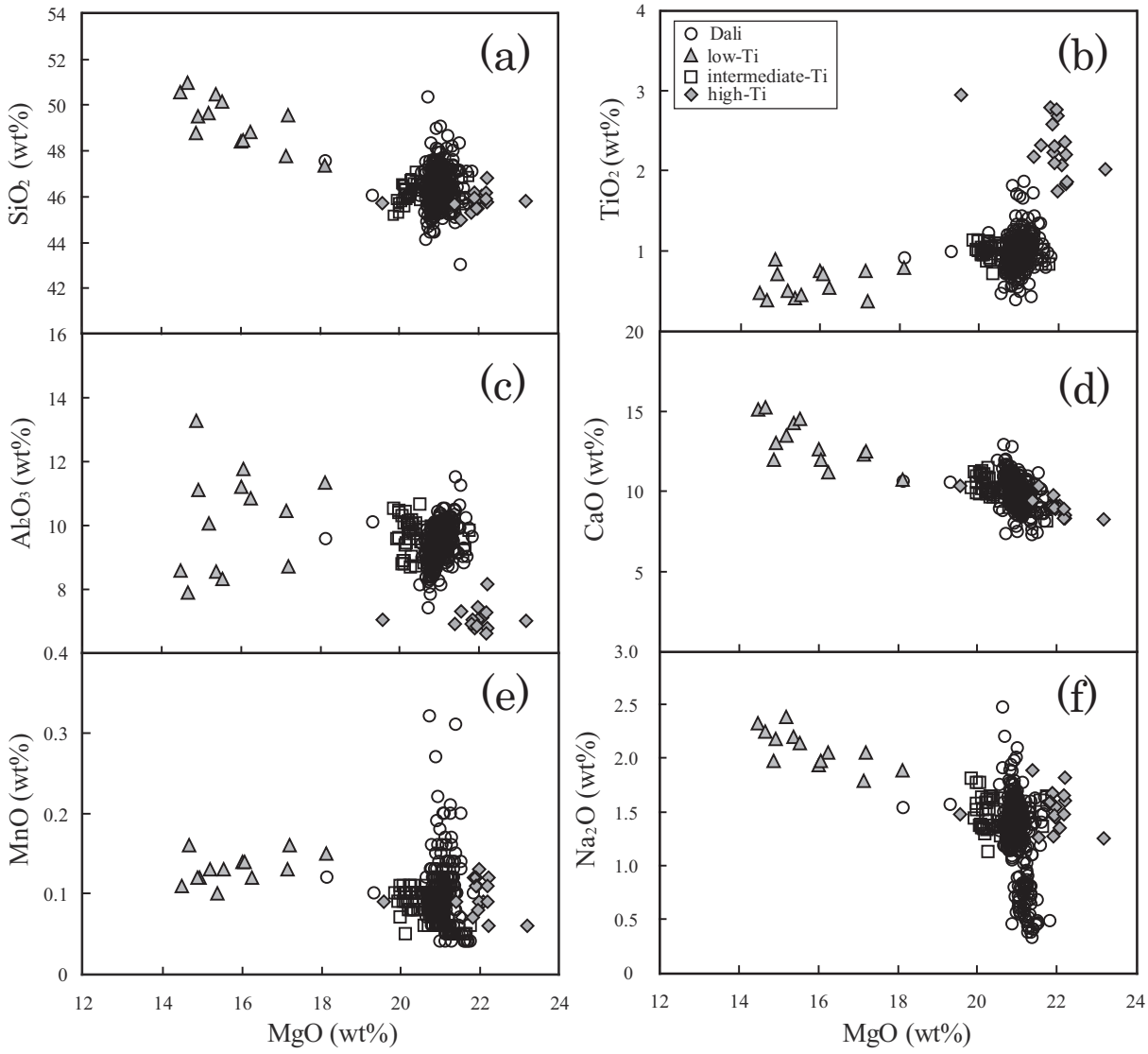

Fig. 10. MgO variation diagrams for the calculated primary magma compositions from the Dali, low-, intermediate- and high-Ti Emeishan melt inclusions. Only corrected melt inclusion data with MgO > 10 wt.% are used in the calculations. The calculated primary magma compositions of the Dali, low-, intermediate- and high-Ti types show systematic compositional variations. See text for explanation.

On the other hand, the MgO contents in the melts are sensitive to pressure during the partial melting of pyroxenite (Kogiso et al., 2003, 2004); higher MgO contents are expected in melts derived from partial melting at higher pressures (see Fig. 2 of Kogiso et al., 1998). It is possible that the MgO (also FeO^T) contents of melt derived from lower degrees of melting at higher pressure may be higher than that of melt derived from higher degrees of melting at lower pressure of the same pyroxenite source (see Table 3 of Kogiso et al., 1998). Thus, the higher TiO_2, MgO and lower SiO_2, Al_2O_3, CaO, in the high-Ti primary magmas compared to those of the low-Ti primary magmas imply that the high-Ti magmas were generated by lower degrees of melting at greater depth than the low-Ti magmas.

The greater enrichment of incompatible trace elements (e.g. Rb, Sr, Zr, and Nb) in the high-Ti lavas than those in the low-Ti lavas (Fig. 11) is also consistent with the former being generated by lower degrees of partial melting. The higher Yb and Lu abundances in the low-Ti lavas (Fig. 11) imply that the low-Ti lavas were derived from higher degrees of partial melting because Yb and Lu are compatible in garnet. Therefore, high degrees of melting of a garnet-rich source will release Yb and Lu.

Olivines from the low-Ti Emeishan picrites have higher Ca and Mn contents and Fe/Mn than those of the high-Ti olivines from the Emeishan picrites (Fig. 2, Kamenetsky et al., 2012), which mirror those of melt inclusions. Sobolev et al. (2007, 2008) proposed a method that allows the quantitative reconstruction of the amount of the pyroxenite component in the peridotite mantle. This method is based on the coherent variations of Ni and Mn in olivine phenocrysts, reflecting the relative contributions of the pure peridotite mantle and the pyroxenite component (Sobolev et al., 2007, 2008; Gurenko et al., 2010).

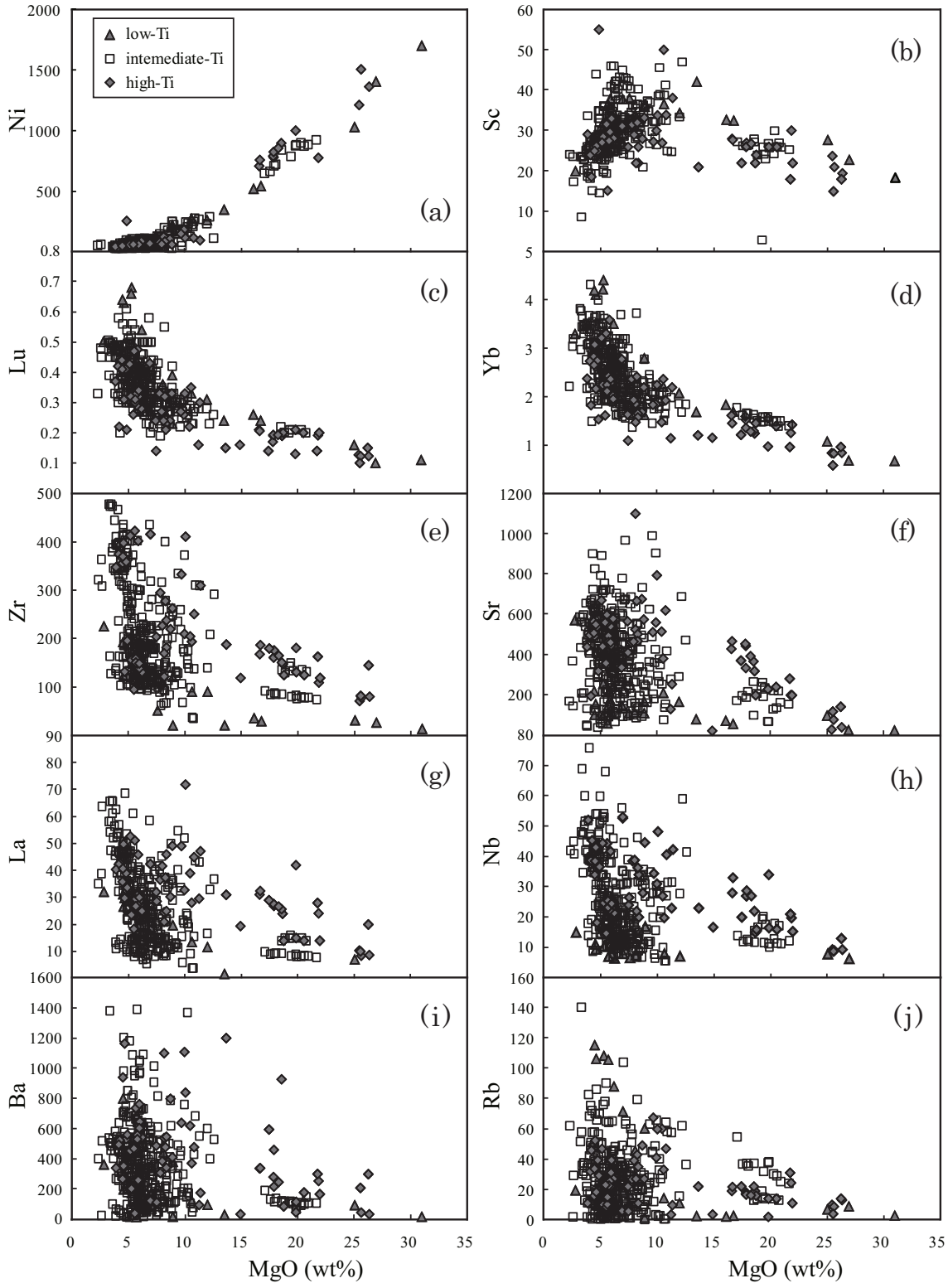

Fig. 11. Variation of trace elements with MgO in the Emeishan basalts. At MgO > 10 wt.%, olivine-compatible Ni, and garnet-compatible Lu and Yb are higher in the low-Ti basalts, whereas incompatible elements Zr, Sr, La, Nb, Ba, and Rb are higher in the high-Ti lavas. Data sources as in Fig. 8.

Kamenetsky et al. (2012) calculated the proportion of the pyroxenite component in the peridotite source for the Emeishan magmas using the method of Sobolev et al. (2008) and Gurenko et al. (2010). The result shows that the mantle sources for the intermediate-Ti magma and high-Ti magma have 21% and 47% of a garnet pyroxenite

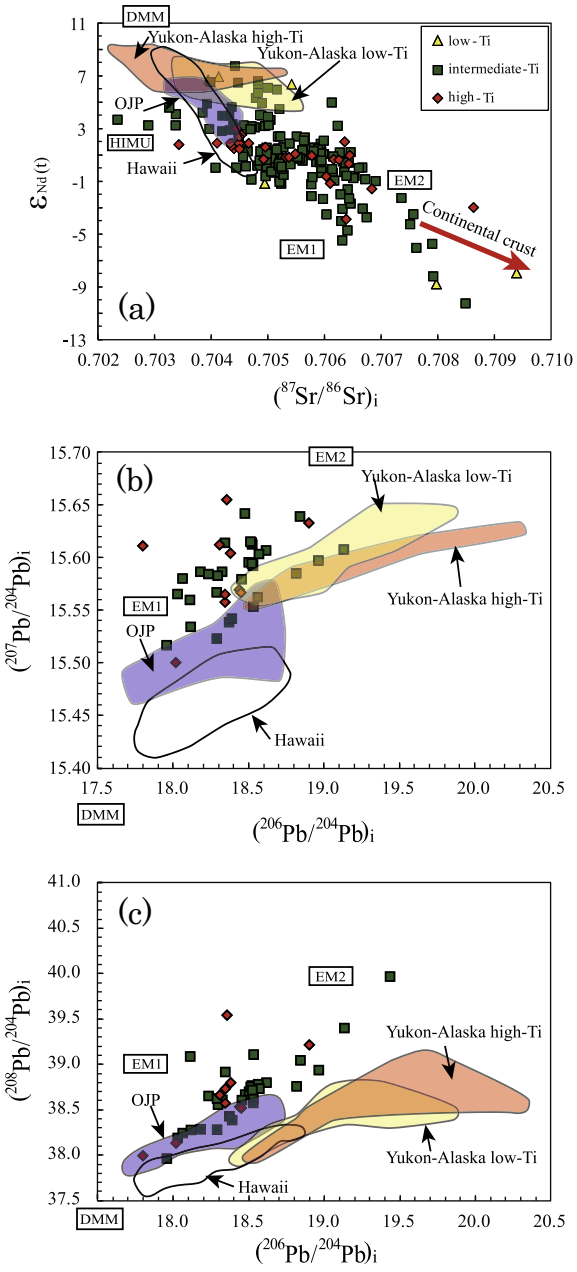

Fig. 12. Initial (a) $^{87}Sr/^{86}Sr$ vs ε_{Nd}, (b) $^{206}Pb/^{204}Pb$ vs $^{207}Pb/^{204}Pb$, and (c) $^{206}Pb/^{204}Pb$ vs $^{208}Pb/^{204}Pb$ for the Emeishan basalts compared to tholeiitic basalts from the OJP, Hawaiian shield and Wrangellia Plateau (Yukon-Alaska low- and high-Ti). Data sources: Emeishan basalts as in Figs. 6 and 9; OJP, Hawaiian shield and Wrangellia Plateau basalts as in Fig. 6. The EM1, EM2, HIMU and DMM end-members are from Hofmann (2003). The trend for continental crust is from Hofmann (1997).

component, respectively. If the diversity in Ni, Mn contents in olivines, as suggested by Kamenetsky et al. (2012), reflects the proportion of pyroxenite component in the peridotite source, then a correlation between Ti_2O/Al_2O_3 ratios and Pb isotopic ratios in melt inclusions from their host olivines is expected, because the incompatibilities of Al for pyroxenite-melt and peridotite-melt are very different, and pyroxenite and peridotite are expected to have different Pb isotope compositions. However, we observed that the TiO_2/Al_2O_3 ratios of the Dali melt inclusions, spanning from the low-, intermediate- to the high-Ti compositions, do not correlate with Pb isotopic ratios (Fig. 7g and h). As discussed before, the compositional diversity of the low-, intermediate- and high-Ti magmas reflects various degrees of melting of a relatively homogeneous source rather than heterogeneous sources.

Nickel partitioning between olivine and melt depends on temperature, pressure, and compositions of the melt. In particular, $D_{Ni}^{Ol/L}$ decreases with increasing MgO content of the melt (Jones, 1984; Beattie et al., 1991). As stated before, the partial melt generated at higher pressure is characterised by higher MgO contents, and then $D_{Ni}^{Ol/L}$ will become lower. As a result, the high-Ti (high-pressure) melts will be expected to have higher Ni contents and low-Ti (low-pressure) melts will have lower Ni contents. Therefore, in the shallower magma chamber(s), olivines crystallized from the high-Ti melts would have higher Ni contents, and that crystallized from the low-Ti melts will have lower Ni contents at a given Fo content. This is consistent with the Ni contents observed in the high-Ti and low-Ti Emeishan picrites (Fig. 2c).

The higher Ca and Mn contents in the low-Ti than high-Ti olivines (Fig. 2) also suggest that they were derived from high-degree melts of a pyroxenite source. High degree melting of a garnet-rich pyroxenite can release Ca and Mn from clinopyroxene and garnet resulting in higher CaO and MnO contents in the melts (Kogiso et al., 1998; Herzberg, 2011).

In summary, as many elements (e.g. Ca, Mn, Al, Yb, and Lu) behave differently during the partial melting of pyroxenite compared to how they would behave during the partial melting of peridotite, the model of melting processes in the Emeishan mantle source proposed here is different from the previous models that are based on melting processes in a peridotite source.

5.5. The origin of the source

The linear arrays of the Pb isotope ratios in the Dali melt inclusions may reflect the results of simple mixing of two mantle components, EM1 and FOZO (Fig. 6). The EM1 component is interpreted to be derived from ancient recycled oceanic crust that includes a small amount of pelagic sediment (e.g., Weaver, 1991; Hauri, 1996; Hofmann, 1997; Lassiter and Hauri, 1998; Blichert-Toft et al., 1999; Stracke et al., 2003). FOZO is a common component from the lower mantle that may be the high $^3He/^4He$ mantle reservoir (Hart et al., 1992). Similar mantle component termed the 'common mantle source' (C) and high $^3He/^4He$ mantle component "PHEM" were proposed by Hanan and Graham (1996) and Farley et al. (1992), respectively. FOZO component represents the common, possibly fed from the deep, lower mantle sampled by many OIBs (Hart et al., 1992; Lee et al., 2010). The result of the isotopic mixing modelling (Fig. 14) shows that the Pb isotopic variation of the melt inclusions could be generated by mixing of different proportions of a recycled ancient oceanic crust component (EM1-like, 10–30%) and a peridotite

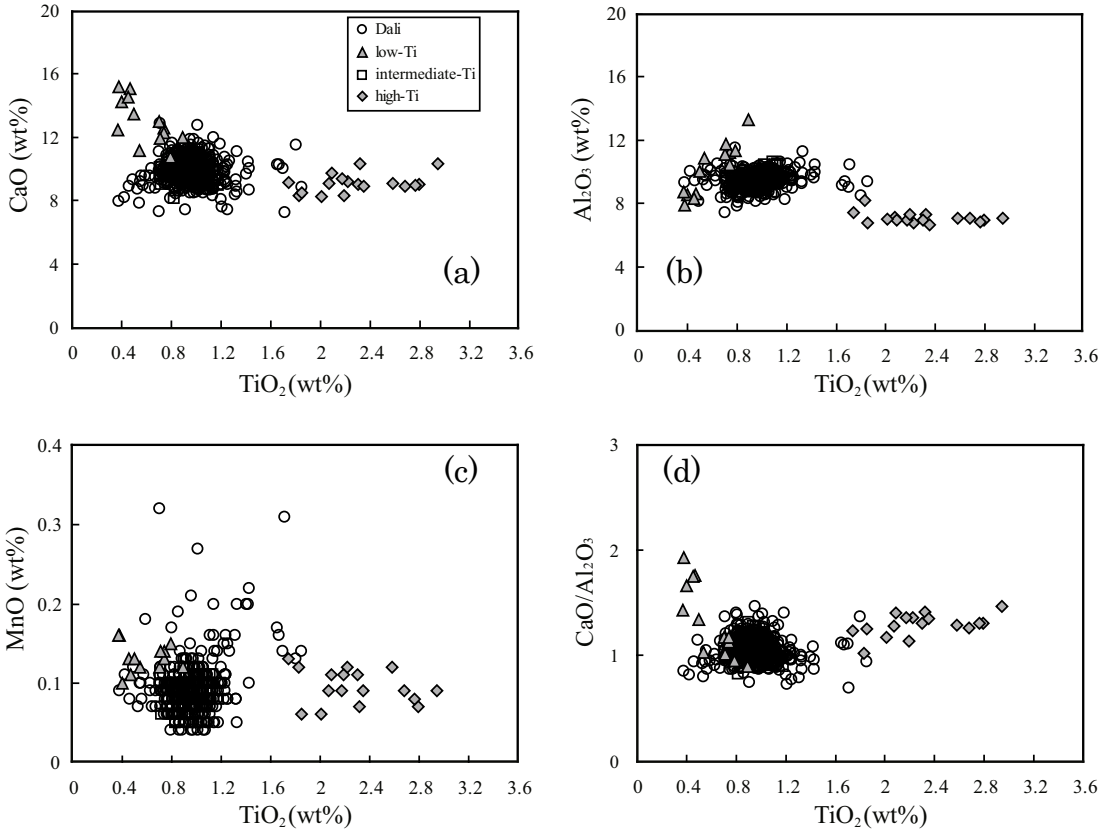

Fig. 13. Variation of (a) CaO, (b) Al_2O_3, (c) MnO, and (d) CaO/Al_2O_3 with TiO_2 in the low-, intermediate- and high-Ti primary magmas and the Dali primary magmas. See text for explanation.

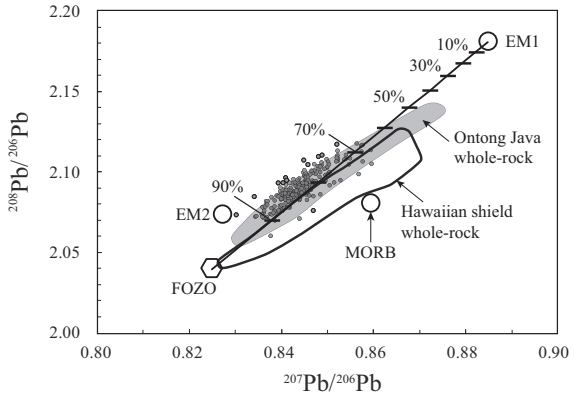

Fig. 14. Pb isotope ratios for melt inclusions from the Dali picrites together with fields of the whole-rock compositions of the OJP and Hawaiian shield basalts. Data sources: OJP and Hawaiian basalts as in Fig. 6; the EM1, EM2, FOZO, and MORB end-members as in Fig. 6. Mixing calculations show that pyroxenites formed by mixing 10–30% of recycled ancient oceanic crust component (EM1) with 90–70% of peridotite component (FOZO) could produce Pb isotope compositions similar to the Emeishan melt inclusions. Mixing lines assume the $^{207}Pb/^{206}Pb$ and $^{208}Pb/^{206}Pb$ of EM1 are 0.885 and 2.18, respectively, and 0.825 and 2.04 for FOZO, respectively (Saal et al., 1998, 2005). The Pb concentrations used for EM1 and FOZO are 0.5 ppm (Weaver, 1991) and 0.2 ppm (Ren et al., 2006), respectively.

component from the lower mantle (FOZO-like component, 70–90%). In addition, most of the Pb isotopic ratios, could be produced by addition of ~15–20% recycled ancient oceanic crust to the peridotite matrix. The Pb isotope compositions of the Dali melt inclusions, which spanning the Emeishan low-, intermediate- and high-Ti basalts, are better to be explained, at present, to be derived from a mixed source; an EM1-like component from recycled oceanic crust plus pelagic sediment, and a FOZO-like component in the form of peridotite from the lower mantle. The trace element characteristics of the Emeishan lavas also support the presence of a recycled oceanic crust component in the Emeishan mantle source. The abundances of immobile trace elements, such as Zr and Nb, are similar to those in OIB but distinct from those in normal MORB (Ali et al., 2010). Ali et al. (2010) calculated the ranges of the Zr contents in the primary Emeishan magma compositions and indicated that the Emeishan mantle source must have been enriched, possibly by the addition of recycled oceanic crust.

The CMAS projection of the Dali primary magmas (Fig. 15) shows that almost all the low-, intermediate- and high-Ti primary magmas are nepheline-normative, falling above the Fo-An join. Additionally, all primary magma compositions fall on the silica-poor side of the En-CaTs join in the Fo-Qtz-CaTs pseudoternary, indicating that a mantle source component that falls on the silica-poor side of the thermal divide was involved in the generation of

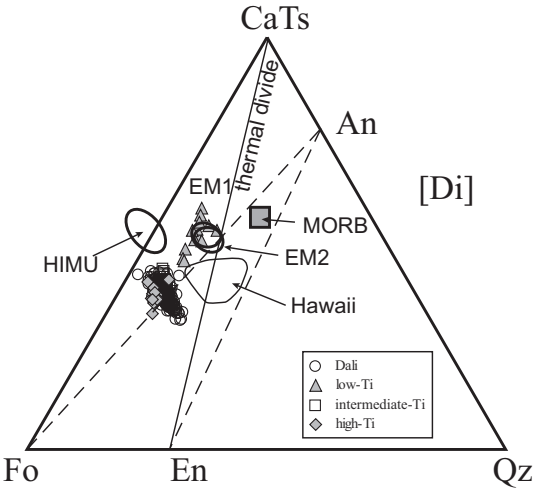

Fig. 15. CMAS projections of O'Hara (1968) showing the normative compositions of the primary magmas for the low-, intermediate- and high-Ti type basalts in the pseudoternary system forsterite (Fo: Mg_2SiO_4)-Ca-Tschermaks (CaTs: $CaAl_2SiO_6$)-quartz (Qtz: SiO_2), projected from diposide [Di]. The plotted primary magma compositions of the Emeishan basalts have MgO contents ranging from 14.5 to 23.2 wt.%. Olivine fractionation corrected average compositions of HIMU, EM1, EM2, MORB and Hawaiian basalts (after Jackson and Dasgupta, 2008) are plotted for reference. See text for further explanation.

the Emeishan basalts (Kogiso et al., 2004; Jackson and Dasgupta, 2008). Fig. 15 also shows that the Emeishan source is different from the HIMU and Hawaii sources, which are SiO_2-poor and SiO_2-rich, respectively. Based on Fig. 15, we speculate that although the Emeishan mantle source and the Hawaii mantle source are pyroxenite and both sources include a recycled oceanic crust component, there is a lower proportion of recycled oceanic crust component and a higher proportion of silica-poor and high-magnesian pyroxenite in the Emeishan source. The differences between the low-Ti and high-Ti primary magmas in the CMAS projections reflect the differences in the compositions of the low-Ti and high-Ti primary magmas, with the latter having higher MgO and FeO^T contents. This is a result of different melting processes in the similar Emeishan mantle sources of the various magma types.

5.6. The origin of the low-Ti and high-Ti magmas and Emeishan mantle plume

The origin of the Emeishan flood basalts has been widely attributed to a mantle plume (Chung and Jahn, 1995; He et al., 2003; Xu et al., 2004; Zhang et al., 2006; Fan et al., 2008; Song et al., 2008b; Ali et al., 2010; Li et al., 2010, 2014). On the basis of the above observations and discussions, we propose a new Emeishan mantle plume model that can explain the geochemical differences of the low-, intermediate- and high-Ti lavas. Our melt inclusion data, together with previous geochemical data, imply that ancient recycled oceanic crust and sediment contributed to a relatively homogeneous pyroxenite source. The ancient recycled oceanic crust and sediment, and surrounding peridotite matrix could have been stirred and well-mixed and underwent solid-state reaction (e.g. Herzberg, 2011) throughout the convective cycle involving the plume head, to create a secondary pyroxenite source, or the reaction might have been be catalysed by small amounts of water and even partial melt in the lower mantle (Vidito et al., 2013). The plume rises from the lower mantle to the upper mantle and melts under garnet-pyroxenite facies conditions as a result of decompression. The partial melts derived by lower degree melting of pyroxenite at greater depths have higher MgO, FeO^T and incompatible element (e.g. Rb, Sr, Zr, and Nb) concentrations, and lower CaO, Al_2O_3 and compatible element (e.g. Yb, Lu, and Mn) concentrations than those of melts derived from high degree of melting at shallower depths.

The compositional variations in the melt inclusions from the Dali picrites, in particular, the presence of low-, intermediate- and high-Ti melt inclusions imply that the Emeishan olivines trapped melts in the magma chamber (s) derived from primary melts that were generated at different depths in the melting column in the mantle source.

6. CONCLUSIONS

Melt inclusions hosted in olivines from the Dali picrites and other picrites within the Emeishan LIP have been used to derive primary magma compositions for the low-, intermediate- and high-Ti Emeishan magma types. Relatively constant Pb isotope ratios among and between the three types in the Dali melt inclusions, the similar isotope compositions from the low-Ti and high-Ti Emeishan picrites together with the very similar incompatible trace element patterns in the clinopyroxenes from other Emeishan picrites belonging to each type, imply that the low-, intermediate- and high-Ti lava types were derived from the melting of a relatively compositionally homogeneous source. The compatible behaviour of the Al_2O_3, CaO, MnO and Yb and the incompatible behaviour of Ti, Rb, Sr, Zr, and Nb during advanced melting imply that the source of the Emeishan mafic lavas is pyroxenite. The higher incompatible trace element contents, and TiO_2, MgO, FeO^T, Ni contents, and lower Al_2O_3, CaO, MnO, Yb and Lu contents in the high-Ti melts compared to those of low-Ti melts reflect lower degrees of melting at greater depths for the high-Ti melts. This new model for the Emeishan mantle plume could explain the geochemical differences of the already recognised low-, intermediate- and high-Ti Emeishan basalts.

ACKNOWLEDGEMENTS

The paper benefited from the constructive comments from F.-Z. Teng, M.L. Tejada, C. Herzberg, N.T. Arndt, D. Weis, and Two anonymous reviewers. The authors gratefully acknowledge the financial support from the Strategic Priority Research Program (B) of the Chinese Academy of Sciences (XDB18030601), National Science Foundation of China (41172064), the National Basic Research Program of China (2011CB808903), and the 'hundred talent project' of Chinese Academy of Sciences.

APPENDIX A. SUPPLEMENTARY MATERIAL

Supplementary data associated with this article can be found, in the online version, at http://dx.doi.org/10.1016/j.gca.2017.01.054.

REFERENCES

Abouchami W., Hofmann A. W., Galer S. J. G., Frey F. A., Eisele J. and Feigenson M. (2005) Lead isotopes reveal bilateral asymmetry and vertical continuity in the Hawaiian mantle plume. *Nature* **434**, 851–856.

Ali J. R., Thompson G. M., Zhou M. F. and Song X. Y. (2005) Emeishan large igneous province, SW China. *Lithos* **79**, 475–489.

Ali J. R., Fitton J. G. and Herzberg C. (2010) Emeishan large igneous province (SW China) and the mantle-plume up-doming hypothesis. *J. Geol. Soc. London* **167**, 953–959.

Beattie P., Ford C. and Russell D. (1991) Partition coefficients for olivine-melt and orthopyroxene-melt systems. *Contrib. Mineral. Petrol.* **109**, 212–224.

Blichert-Toft J., Frey F. A. and Albarede F. (1999) Hf isotope evidence for pelagic sediments in the source of Hawaiian basalts. *Science* **285**, 879–882.

Blichert-Toft J., Weise D., Maerschalk C., Agranier A. and Albare'de F. (2003) Hawaiian hot spot dynamics as inferred from the Hf and Pb isotope evolution of Mauna Kea volcano. *Geochem. Geophys. Geosyst.* **4**(2). http://dx.doi.org/10.1029/2002GC000340.

Charlier B., Namur O., Toplis M. J., Schiano P., Cluzel N., Higgins M. D. and Vander Auwera J. (2011) Large-scale silicate liquid immiscibility during differentiation of tholeiitic basalt to granite and the origin of the Daly gap. *Geology* **39**, 907–910.

Chung S. L. and Jahn B. M. (1995) Plume-lithosphere interaction in generation of the Emeishan flood basalts at the Permian-Triassic boundary. *Geology* **23**, 889–892.

Chung, S.L., Jahn, B.M., Genyao, W., Lo, C.H., Bolin, C., 1998. The Emeishan flood Basalt in SW China: a mantle plume initiation model and its connection with continental breakup and mass extinction at the Permian-Triassic boundary. In: Flower, M.F.J., Chung, S.L., Lo, C.H., Lee, T.Y. (Eds.), Mantle Dynamics and Plate Interactions in East Asia AGU Geodyn, Ser. vol. 27, AGU, Washington, DC, pp. 47–58.

Coffin M. F. and Eldholm O. (1994) Large igneous provinces: crustal structure, dimension, and external consequences. *Rev. Geophys.* **32**, 1–36.

Coombs M. L., Clague D. A., Moore F. F. and Cousens B. L. (2004) Growth and collapse of Waianae Volcano, Hawaii, as revealed by exploration of its submarine flanks. *Geochem. Geophys. Geosyst.* **5**. http://dx.doi.org/10.1029/2004GC000717.

Danyushevsky L. V., Della-Pasqua F. N. and Sokolov S. (2000) Re-equilibration of melt inclusions trapped by magnesian olivine phenocrysts from subduction-related magmas: petrological implications. *Contrib. Mineral. Petrol.* **138**, 68–83.

Danyushevsky L. V., McNeill A. W. and Sobolev A. V. (2002) Experimental and petrological studies of melt inclusions in phenocrysts from mantle-derived magmas: an overview of techniques, advantages and complications. *Chem. Geol.* **183**, 5–24.

Danyushevsky L. V. and Plechov P. (2011) Petrolog 3: integrated software for modeling crystallization processes. *Geochem. Geophys. Geosyst.* **12**. http://dx.doi.org/10.1029/2011GC003516.

Eisele J., Abouchami W., Galer S. J. G. and Hofmann A. W. (2003) The 320 kyr Pb isotope evolution of Mauna Kea lavas recorded in the HSDP-2 drill core. *Geochem. Geophys. Geosyst.* **4**(5), 8710. http://dx.doi.org/10.1029/2002GC000339.

Fan W., Zhang C., Wang Y., Guo F. and Peng T. (2008) Geochronology and geochemistry of Permian basalts in western Guangxi Province, Southwest China: evidence for plume-lithosphere interaction. *Lithos* **102**, 218–236.

Farley K. A., Natland J. H. and Craig H. (1992) Binary mixing of enriched and undegassed (primitive?) mantle components (He, Sr, Nd, Pb) in Samoan lavas. *Earth Planet. Sci. Lett.* **111**, 183–199.

Fekiacova Z., Abouchami W., Galer S. J. G., Garcia M. O. and Hofmann A. W. (2007) Origin and temporal evolution of Ko'olau Volcano, Hawai'i: inferences from isotope data on the Ko'olau Scientific Drilling Project (KSDP), the Honolulu Volcanics and ODP Site 843. *Earth Planet. Sci. Lett.* **261**, 65–83.

Frey F. A., Clague D., Mahoney J. J. and Sinton J. M. (2000) Volcanism at the edge of the Hawaiian plume: petrogenesis of submarine alkalic lavas from the North ArchVolcanic Field. *J. Petrol.* **41**, 667–691.

Ford C. E., Russel D. G., Craven J. A. and Fisk M. R. (1983) Olivine-liquid equilibria: temperature, pressure and composition dependence of the crystal/liquid cation partition coefficients for Mg, Fe^{2+}, Ca and Mn. *J. Petrol.* **24**, 256–265.

Garcia M. O., Swinnard L., Weis D., Greene A. R., Tagami T., Sano H. and Gandy C. E. (2010) Petrology, geochemistry and geochronology of Kaua'I lavas over 4.5 Myr: implications for the origin of rejuvenated volcanism and the evolution of the Hawaiian plume. *J. Petrol.* **51**, 1507–1540.

Greene A. R., Scoates J. S. and Weis D. (2008) Wrangellia flood basalts in Alaska: a record of plume-lithosphere interaction in a Late Triassic accreted oceanic plateau. *Geochem. Geophys. Geosyst.* **9**. http://dx.doi.org/10.1029/2008GC002092.

Greene A. R., Scoates J. S., Weis D. and Israel S. (2009a) Geochemistry of Triassic flood basalts from the Yukon (Canada) segment of the accreted Wrangellia oceanic plateau. *Lithos* **110**, 1–19.

Greene A. R., Scoates J. S., Weis D., Nixon G. T. and Kieffer B. (2009b) Melting history and magmatic evolution of basalts and picrites from the accreted Wrangellia Oceanic Plateau, Vancouver Island, Canada. *J. Petrol.* **50**, 467–505.

Gurenko A. A., Hoernle K. A., Sobolev A. V., Hauff F. and Schmincke H. U. (2010) Source components of the Gran Canaria (Canary Islands) shield stage magmas: evidence from olivine composition and Sr-Nd-Pb isotopes. *Contrib. Mineral. Petrol.* **159**, 689–702.

Hanan B. B. and Graham D. W. (1996) Lead and helium isotope evidence from oceanic basalts for a common deep source of mantle plumes. *Science* **272**, 991–995.

Hanski E., Walker R. J., Huhma H., Polyakov G. V., Balykin P. A., Trong H. T. and Thi P. N. (2004) Origin of the Permo-Triassic komatiites, northwestern Vietnam. *Contrib. Mineral. Petrol.* **147**, 453–469.

Hanski E., Kamenetsky V. S., Luo Z. Y., Xu Y. G. and Kuzmin D. V. (2010) Primitive magmas in the Emeishan Large Igneous Province, southwestern China and northern Vietnam. *Lithos* **119**, 75–90.

Hart S. R., Hauri E. H. and Oschmann L. A. (1992) Mantle plumes and entrainment: isotope evidence. *Science* **256**, 517–520.

Hauri E. H. (1996) Major-element variability in the Hawaiian mantle plume. *Nature* **382**, 415–419.

Hauri E. H. (2002) SIMS analysis of volatiles in silicate glasses, 2: isotopes and abundances in Hawaiian melt inclusions. *Chem. Geol.* **183**, 115–141.

He B., Xu Y. G., Chung S. L., Xiao L. and Wang Y. (2003) Sedimentary evidence for a rapid, kilometer-scale crustal

doming prior to the eruption of the Emeishan flood basalts. *Earth Planet. Sci. Lett.* **213**, 391–405.

He B., Xu Y. G., Huang X. L., Luo Z. Y., Shi Y. R., Yang Q. J. and Yu S. Y. (2007) Age and duration of the Emeishan flood volcanism, SW China: geochemistry and SHRIMP zircon U-Pb dating of silicic ignimbrites, post-volcanic Xuanwei Formation and clay tuff at the Chaotian section. *Earth Planet. Sci. Lett.* **255**, 306–323.

Herzberg C. (2006) Petrology and thermal structure of the Hawaiian plume from Mauna Kea volcano. *Nature* **444**, 605–609.

Herzberg C. (2011) Identification of source lithology in the hawaiian and canary islands: implications for origins. *J. Petrol.* **52**, 113–146.

Hofmann A. W. (1997) Mantle geochemistry: the message from oceanic volcanism. *Nature* **385**, 219–229.

Hofmann A. W. (2003) Sampling mantle heterogeneity through oceanic basalts: isotopes and trace elements. In *Treatise on Geochemistry* (eds. H. D. Holland and K. K. Turekian). Pergamon, Oxford, pp. 61–101.

Hong L. B., Zhang Y. H., Qian S. P., Liu J. Q., Ren Z. Y. and Xu Y. G. (2013) Constraints from melt inclusions and their host olivines on the petrogenesis of Oligocene-Early Miocene Xindian basalts, Chifeng area, North China Craton. *Contrib. Mineral. Petrol.* **165**, 305–326.

Hou T., Zhang Z., Kusky T., Du Y., Liu J. and Zhao Z. (2011) A reappraisal of the high-Ti and low-Ti classification of basalts and petrogenetic linkage between basalts and mafic–ultramafic intrusions in the Emeishan Large Igneous Province, SW China. *Ore Geol. Rev.* **41**, 133–143.

Hou T., Zhang Z. C., Encarnacion J., Santosh M. and Sun Y. L. (2013) The role of recycled oceanic crust in magmatism and metallogeny: Os-Sr-Nd isotopes, U-Pb geochronology and geochemistry of picritic dykes in the Panzhihua giant Fe-Ti oxide deposit, central Emeishan large igneous province, SW China. *Contrib. Mineral. Petrol.* **165**, 805–822.

Jackson M. G. and Dasgupta R. (2008) Compositions of HIMU, EM1, and EM2 from global trends between radiogenic isotopes and major elements in ocean island basalts. *Earth Planet. Sci. Lett.* **276**, 175–186.

Jones D. L., Silberling N. J. and Hillhouse J. (1977) Wrangellia-a displaced terrane in northwestern North America. *Can. J. Earth Sci.* **14**, 2565–2577.

Jones J. H. (1984) Temperature and pressure-independent correlations of olivine-liquid partition coefficients and their application to trace element partitioning. *Contrib. Mineral. Petrol.* **88**, 126–132.

Kamenetsky V. S., Crawford A. J., Eggins S. and Mühe R. (1997) Phenocryst and melt inclusion chemistry of near-axis seamounts, Valu Fa Ridge, Lau Basin: insight into mantle wedge melting and the addition of subduction components. *Earth Planet. Sci. Lett.* **151**, 205–223.

Kamenetsky V. S., Chung S. L., Kamenetsky M. B. and Kuzmin D. V. (2012) Picrites from the Emeishan Large Igneous Province, SW China: a compositional continuum in primitive magmas and their respective mantle sources. *J. Petrol.* **53**, 2095–2113.

Kent A. J. R., Norman M. D., Hutcheon I. D. and Stolper E. M. (1999) Assimilation of seawater-derived components in an oceanic volcano: evidence from matrix glasses and glass inclusions from Loihi seamount, Hawaii. *Chem. Geol.* **156**, 299–319.

Kent A. J., Baker J. A. and Wiedenbeck M. (2002) Contamination and melt aggregation processes in continental flood basalts: constraints from melt inclusions in Oligocene basalts from Yemen. *Earth. Planet. Sci. Lett.* **202**, 577–594.

Kent A. J. R. (2008) Melt inclusions in basaltic and related volcanic rocks. *Rev. Mineral. Geochem.* **69**, 273–331.

Kimura J., Sisson T. W., Nakano N., Coombs M. L. and Lipman P. W. (2006) Isotope geochemistry of early Kilauea magmas from the submarine Hilina bench: the nature of the Hilina mantle component. *J. Volcanol. Geotherm. Res.* **151**, 51–72.

Kogiso T., Hirose K. and Takahashi E. (1998) Melting experiments on homogeneous mixtures of peridotite and basalt: application to the genesis of ocean island basalts. *Earth Planet. Sci. Lett.* **162**, 45–61.

Kogiso T., Hirschmann M. M. and Frost D. J. (2003) High-pressure partial melting of garnet pyroxenite: possible mafic lithologies in the source of ocean island basalts. *Earth Planet. Sci. Lett.* **216**, 603–617.

Kogiso T., Hirschmann M. M. and Pertermann M. (2004) High-pressure partial melting of mafic lithologies in the mantle. *J. Petrol.* **45**, 2407–2422.

Lai S. C., Qin J. F., Li Y. F., Li S. Z. and Santosh M. (2012) Permian high Ti/Y basalts from the eastern part of the Emeishan Large Igneous Province, southwestern China: petrogenesis and tectonic implications. *J. Asian Earth Sci.* **47**, 216–230.

Lassiter J. C. and Hauri E. H. (1998) Osmium-isotope variations in Hawaiian lavas: evidence for recycled oceanic lithosphere in the Hawaiian plume. *Earth Planet. Sci. Lett.* **164**, 483–496.

Le Bas M. J., Le Maitre R. W., Streckeisen A. and Zanettin B. (1986) A chemical classification of volcanic rocks based on the total alkali-silica diagram. *J. Petrol.* **27**, 745–750.

Lee C. T., Luffi P., Hoink T., Li J., Dasgupta R. and Hernlund J. (2010) Upside-down differentiation and generation of a 'primordial' lower mantle. *Nature* **463**, 930–935.

Li J., Xu J. F., Suzuki K., He B., Xu Y. G. and Ren Z. Y. (2010) Os, Nd and Sr isotope and trace element geochemistry of the Muli picrites: insights into the mantle source of the Emeishan Large Igneous Province. *Lithos* **119**, 108–122.

Li J., Wang X. C., Ren Z. Y., Xu J. F., He B. and Xu Y. G. (2014) Chemical heterogeneity of the Emeishan mantle plume: evidence from highly siderophile element abundances in picrites. *J. Asian Earth Sci.* **79**, 191–205.

Liu C. and Zhu R. (2009) Geodynamic significances of the Emeishan basalts. *Earth Sci. Front.* **16**, 52–69.

Liu J. Q., Ren Z. Y., Nichols A. R., Song M. S., Qian S. P., Zhang Y. and Zhao P. P. (2015) Petrogenesis of Late Cenozoic basalts from North Hainan Island: constraints from melt inclusions and their host olivines. *Geochim. Cosmochim. Acta* **152**, 89–121.

Liu P. P., Zhou M. F., Ren R. Z., Wang C. Y. and Wang K. (2016) Immiscible Fe- and Si-rich silicate melts in plagioclase from the Baima mafic intrusion (SW China): implications for the origin of bi-modal igneous suites in large igneous provinces. *J. Asian Earth Sci.* **127**, 211–230.

Lo C. H., Chung S. L., Lee T. Y. and Wu G. Y. (2002) Age of the Emeishan flood magmatism and relations to Permian-Triassic boundary events. *Earth Planet. Sci. Lett.* **198**, 449–458.

Maclennan J. (2008) Concurrent mixing and cooling of melts under Iceland. *J. Petrol.* **49**, 1931–1953.

Mahoney, J.J., 1987. An isotopic survey of Pacific oceanic plateaus: Implications for their nature and origin. In: Keating, B.H., Fryer, P., Batiza, R., Boehlert, G.W. (Eds.), American Geophysical Union Monograph 43, Washington, DC, pp. 207–220.

Mahoney, J.J., Storey, M., Duncan, R.A., Spencer, K.J., Pringle, M., 1993a. Geochemistry and age of the Ontong Java Plateau. In: Pringle, M.S., Sager, W.W., Sliter, W.V., Stein, S. (Eds.), Geophysical Monograph, vol. 77. American Geophysical Union, Washington, pp. 233–261.

Mahoney, J.J., Storey, M., Duncan, R.A., Spencer, K.J., Pringle, M., 1993b. Geochemistry and geochronology of Leg 130

basement lavas: nature and origin of the Ontong Java Plateau. In: Berger, W.H., Kroenke, L.W., Mayer, L.A. (Eds.), Proc. ODP. Sci. Results, vol. 130, pp. 3–22.

Mahoney, J.J., Coffin, M.F. (Eds.), 1997 Large Igneous Provinces: Continental, Oceanic and Planetary Flood Volcanism. American Geophysical Union Monograph 100, AGU, Washington, DC, 438.

Marske J. P., Pietruszka A. J., Weis D., Garcia M. O. and Rhodes J. M. (2007) Rapid passage of a small-scale mantle heterogeneity through the melting regions of Kilauea and Mauna Loa Volcanoes. *Earth Planet. Sci. Lett.* **259**, 34–50.

Nielsen R. L., Crum J., Bourgeois R., Hascall K., Forsythe L. M., Fisk M. R. and Christie D. M. (1995) Melt inclusions in high-An plagioclase from the Gorda Ridge: an example of the local diversity of MORB parent magmas. *Contrib. Mineral. Petrol.* **122**, 34–50.

Nielsen R. L., Sours-Page R. and Harpp K. (2000) Role of a Cl-bearing flux in the origin of depleted ocean floor magmas. *Geochem. Geophys. Geosys.* **1**, 1999GC000017.

Norman M. D., Garcia M. O., Kamenetsky V. S. and Nielsen R. L. (2002) Olivine-hosted melt inclusions in Hawaiian picrites: equilibration, melting, and plume source characteristics. *Chem. Geol.* **183**, 143–168.

O'hara M. J. (1968) The bearing of phase equilibria studies in synthetic and natural systems on the origin and evolution of basic and ultrabasic rocks. *Earth Sci. Rev.* **4**, 69–133.

Paul B., Woodhead J. D., Hergt J., Danyushevsky L., Kunihiro T. and Nakamura E. (2011) Melt inclusion Pb-isotope analysis by LA-MC-ICPMS: assessment of analytical performance and application to OIB genesis. *Chem. Geol.* **289**, 210–223.

Pertermann M. and Hirschmann M. M. (2002) Trace-element partitioning between vacancy-rich eclogistic clinopyroxene and silicate melt. *Am. Mineral.* **87**, 1365–1376.

Philpotts A. R. and Ague J. J. (2009) *Principles of Igneous and Metamorphic Petrology*, second ed. Cambridge University Press.

Pietruszka A. J. and Garcia M. O. (1999) A rapid fluctuation in the mantle source and melting history of Kilauea Volcano inferred from the geochemistry of its historical summit lavas (1790–1982). *J. Petrol.* **40**, 1321–1342.

Putirka K. D., Perfit M., Ryerson F. J. and Jackson M. G. (2007) Ambient and excess mantle temperatures, olivine thermometry, and active vs. passive upwelling. *Chem. Geol.* **241**, 177–206.

Qi L., Wang C. Y. and Zhou M. F. (2008) Controls on the PGE distribution of Permian Emeishan alkaline and peralkaline volcanic rocks in Longzhoushan, Sichuan Province, SW China. *Lithos* **106**, 222–236.

Qian S. P., Ren Z. Y., Zhang L., Hong L. B. and Liu J. Q. (2015) Chemical and Pb isotope composition of olivine-hosted melt inclusions from the Hannuoba basalts, North China Craton: implications for petrogenesis and mantle source. *Chem. Geol.* **401**, 111–125.

Ren Z. Y., Takahashi E., Orihashi Y. and Johnson K. T. M. (2004) Petrogenesis of tholeiitic lavas from the submarine Hana Ridge, Haleakala Volcano, Hawaii. *J. Petrol.* **45**, 2067–2099.

Ren Z. Y., Ingle S., Takahashi E., Hirano N. and Hirata T. (2005) The chemical structure of the Hawaiian mantle plume. *Nature* **436**, 837–840.

Ren Z. Y., Shibata T., Yoshikawa M., Johnson K. T. M. and Takahashi E. (2006) Isotope Compositions of submarine Hana Ridge, Haleakala Volcano, Hawaii: melting process and the structure of the Hawaiian Plume. *J. Petrol.* **47**, 255–275.

Ren Z. Y., Hanyu T., Miyazaki T., Chang Q., Kawabata H., Takahashi T., Hirahara Y., Nichols R. L. and Tatsumi Y. (2009) Geochemical differences of the Hawaiian shield lavas: implications for melting processes in the heterogeneous Hawaiian plume. *J. Petrol.* **50**, 1553–1573.

Saal A. E., Hart S. R., Shimizu N., Hauri E. H. and Layne G. D. (1998) Pb isotopic variability in melt inclusions from oceanic island basalts, Polynesia. *Science* **282**, 1481–1484.

Saal A. E., Hart S. R., Shimizu N., Hauri E. H., Layne G. D. and Eiler J. M. (2005) Pb isotopic variability in melt inclusions from the EMI - EMII - HIMU mantle end-members and the role of the oceanic lithosphere. *Earth Planet. Sci. Lett.* **240**, 605–620.

Shellnutt J. G., Zhou M. F., Yan D. P. and Wang Y. B. (2008) Longevity of the Permian Emeishan mantle plume (SW China): 1 Ma, 8 Ma or 18 Ma? *Geol. Mag.* **145**, 373–388.

Shellnutt J. G., Usuki T., Kennedy A. K. and Chiu H.-Y. (2015) A lower crust origin of some flood basalts of the Emeishan large igneous province, SW China. *J. Asian Earth Sci.* **109**, 74–85.

Slater L., McKenzie D., Gronvold K. and Shimizu N. (2001) Melt generation and movement beneath Theistareykir, NE Iceland. *J. Petrol.* **42**, 321–354.

Sobolev A. V. and Shimizu N. (1993) Ultra-depleted primary melt included in an olivine from the Mid-Atlantic ridge. *Nature* **363**, 151–154.

Sobolev A. V. (1996) Melt inclusions in minerals as a source of principle petrological information. *Petrology* **4**, 209–220.

Sobolev A. V., Hofmann A. W. and Nikogosian I. K. (2000) Recycled oceanic crust observed in 'ghost plagioclase' within the source of Mauna Loa lavas. *Nature* **404**, 986–990.

Sobolev A. V., Hofmann A. W., Sobolev S. V. and Nikogosian I. K. (2005) An olivine-free mantle source of Hawaiian shield basalts. *Nature* **434**, 590–597.

Sobolev A. V., Hofmann A. W., Kuzmin D. V., Yaxley G. M., Arndt N. T., Chung S. L., Danyushevsky L. V., Elliott T., Frey F. A., Garcia M. O., Gurenko A. A., Kamenetsky V. S., Kerr A. C., Krivolutskaya N. A., Matvienkov V. V., Nikogosian I. K., Rocholl A., Sigurdsson I. A., Sushchevskaya N. M. and Teklay M. (2007) The amount of recycled crust in sources of mantle-derived melts. *Science* **316**, 412–417.

Sobolev A. V., Hofmann A. W., Brugmann G., Batanova V. G. and Kuzmin D. V. (2008) A quantitative link between recycling and osmium isotopes. *Science* **321**, 536-536.

Song X. Y., Zhou M. F., Cao Z. M. and Robinson P. T. (2004) Late Permian rifting of the South China Craton caused by the Emeishan mantle plume? *J. Geol. Soc. London* **161**, 773–781.

Song X. Y., Zhou M. F., Keays R. R., Cao Z. M., Sun M. and Qi L. (2006) Geochemistry of the Emeishan flood basalts at Yangliuping, Sichuan, SW China: implications for sulfide segregation. *Contrib. Mineral. Petrol.* **152**, 53–74.

Song X. Y., Zhou M. F., Tao Y. and Xiao J. F. (2008a) Controls on the metal compositions of magmatic sulfide deposits in the Emeishan large igneous province, SW China. *Chem. Geol.* **253**, 38–49.

Song X. Y., Qi H. W., Robinson P. T., Zhou M. F., Cao Z. M. and Chen L. M. (2008b) Melting of the subcontinental lithospheric mantle by the Emeishan mantle plume; evidence from the basal alkaline basalts in Dongchuan, Yunnan, Southwestern China. *Lithos* **100**, 93–111.

Sours-Page R., Johnson K. T., Nielsen R. L. and Karsten J. L. (1999) Local and regional variation of MORB parent magmas: evidence from melt inclusions from the Endeavour Segment of the Juan de Fuca Ridge. *Contrib. Mineral. Petrol.* **134**, 342–363.

Stanley S. M. and Yang X. (1994) A double mass extinction at the end of the Paleozoic Era. *Science* **266**, 1340–1344.

Stracke A., Bizimis M. and Salters V. J. M. (2003) Recycling oceanic crust: quantitative constraints. *Geochem. Geophys. Geosyst.* **4**, 8003. http://dx.doi.org/10.1029/2001GC000223.

Sun W. D., Bennett V. C., Eggins S. M., Kamenetsky V. S. and Arculus R. J. (2003) Enhanced mantle-to-crust rhenium transfer in undegassed arc magmas. *Nature* **422**, 294–297.

Tanaka, R., Nakamura, E., Takahashi, E., 2002. Geochemical evolution of Koolau Volcano, Hawaii. In: Takahashi, E., Lipman, P.W., Garcia, M.O., Naka, J., Aramaki, S. (Eds.), Hawaiian Volcanoes: Deep Underwater Perspectives, vol. 128. Geophysical Monograph, American Geophysical Union, Washington, DC, pp. 311–332.

Tanaka R., Makishima A. and Nakamura E. (2008) Hawaiian double volcanic chain triggered by an episodic involvement of recycled material: constraints from temporal Sr-Nd-Hf-Pb isotopic trend of the Loa-type volcanoes. *Earth Planet. Sci. Lett.* **265**, 450–465.

Takahashi, E., Nakajima, K., 2002. Melting process in the Hawaiian plume: an experimental study. In: Takahashi, E., Lipman, P.W., Garcia, M.O., Naka, J., Aramaki, S. (Eds.), Hawaiian Volcanoes: Deep Underwater Perspectives, vol. 128. Geophysical Monograph, American Geophysical Union, Washington, DC, pp. 403–418.

Tejada M. L. G., Mahoney J. J., Duncan R. A. and Hawkins M. P. (1996) Age and geochemistry of basement and alkalic rocks of Maliata and Santa Isabel, Solomon Islands, southern margin of Ontong Java Plateau. *J. Petrol.* **37**, 361–394.

Tejada M. L. G., Mahoney J. J., Neal C. R., Duncan R. A. and Petterson M. G. (2002) Basement geochemistry and geochronology of central Malaita, Solomon Islands, with implications for the origin and evolution of the Ontong Java Plateau. *J. Petrol.* **43**, 449–484.

Tejada, M.L.G., Mahoney, J.J., Castillo, P.R., Ingle, S.P., Sheth, H.C., Weis, D., 2004. Pin-pricking the elephant: Evidence on the origin of the Ontong Java Plateau from Pb-Sr-Hf-Nd isotopic characteristics of ODP Leg 192 basalts. In: Fitton, J. G., Mahoney, J.J., Wallace, P.J., Saunders, A.D. (Eds.), Origin and Evolution of the Ontong Java Plateau, vol. 229. Geological Society Special Publication, Geological Society of London, pp. 133–150.

Tejada M. L. G., Suzuki K., Hanyu T., Mahoney J. J., Ishikawa A., Tatsumi Y., Chang Q. and Nakai S. (2013) Cryptic lower crustal signature in the source of the Ontong Java Plateau revealed by Os and Hf isotopes. *Earth Planet. Sci. Lett.* **377**, 86–96.

Thompson R. N. and Gibson S. A. (2000) Transient high temperatures in mantle plume heads inferred from magnesian olivines in Phanerozoic picrites. *Nature* **407**, 502–506.

Tuff J., Takahashi E. and Gibson S. A. (2005) Experimental constraints on the role of garnet pyroxenite in the genesis of high-Fe mantle plume derived melts. *J. Petrol.* **46**, 2023–2058.

Vidito C., Herzberg C., Gazel E., Geist D. and Harpp K. (2013) Lithological structure of the Galapagos Plume. *Geochem. Geophys. Geosyst.* **14**. http://dx.doi.org/10.1002/ggge.20270.

Walter M. J. (1998) Melting of garnet peridotite and the origin of komatiite and depleted lithosphere. *J. Petrol.* **39**, 29–60.

Wang C. Y., Zhou M. F. and Qi L. (2007) Permian flood basalts and mafic intrusions in the Jinping (SW China) Song Da (northern Vietnam) district: mantle sources, crustal contamination and sulfide segregation. *Chem. Geol.* **243**, 317–343.

Wang Z. and Gaetani G. A. (2008) Partitioning of Ni between olivine and siliceous eclogite partial melt: experimental constraints on the mantle source of Hawaiian basalts. *Contrib. Mineral. Petrol.* **156**, 661–678.

Wang C. Y., Zhou M. F. and Zhao D. (2008) Fe-Ti-Cr oxides from the Permian Xinjie mafic–ultramafic layered intrusion in the Emeishan large igneous province, SW China: crystallization from Fe- and Ti-rich basaltic magmas. *Lithos* **102**, 198–217.

Wang C. Y., Zhou M. F., Yang S., Qi L. and Sun Y. (2014) Geochemistry of the Abulangdang intrusion: cumulates of high-Ti picritic magmas in the Emeishan large igneous province, SW China. *Chem. Geol.* **378**, 24–39.

Wanless V. D., Garcia M. O., Trusdell F. A., Rhodes J. M., Norman M. D., Weis D., Fornari D. J., Kurz M. D. and Guillou H. (2006) Submarine radial vents on Mauna Loa Volcano, Hawai'i. *Geochem. Geophys. Geosyst.* **7**. http://dx.doi.org/10.1029/2005GC001086.

Weaver B. L. (1991) The origin of ocean island basalt end-member compositions: trace element and isotopic constraints. *Earth Planet. Sci. Lett.* **104**, 381–397.

Weis D., Kieffer B., Maerschalk C., Pretorius W. and Barling J. (2005) High-precision Pb-Sr-Nd-Hf isotopic characterization of USGS BHVO-1 and BHVO-2 reference materials. *Geochem. Geophys. Geosyst.* **6**. http://dx.doi.org/10.1029/2004gc000852.

Weis D., Garcia M. O., Rhodes J. M., Jellinek M. and Scoates J. S. (2011) Role of the deep mantle in generating the compositional asymmetry of the Hawaiian mantle plume. *Nat. Geosci.* **4**, 831–838.

Wignall P. B., Sun Y., Bond D. P., Izon G., Newton R. J., Vedrine S., Widdowson M., Ali J. R., Lai X., Jiang H., Cope H. and Bottrell S. H. (2009) Volcanism, mass extinction, and carbon isotope fluctuations in the Middle Permian of China. *Science* **324**, 1179–1182.

Xiao L., Xu Y. G., Chung S. L., He B. and Mei H. J. (2003) Chemostratigraphic correlation of Upper Permian lavas from Yunnan province, China: extent of the Emeishan Large Igneous Province. *Int. Geol. Rev.* **45**, 753–766.

Xiao L., Xu Y. G., Mei H. J., Zheng Y. F., He B. and Pirajno F. (2004) Distinct mantle sources of low-Ti and high-Ti basalts from the western Emeishan large igneous province, SW China: implications for plume–lithosphere interaction. *Earth Planet. Sci. Lett.* **228**, 525–546.

Xu Y. G. and Chung S. L. (2001) The Emeishan Large Igneous Province: evidence for mantle plume activity and melting conditions. *Geochimica* **30**, 1–9 (in Chinese with English abstract).

Xu Y. G., Chung S. L., Jahn B. M. and Wu G. Y. (2001) Petrologic and geochemical constraints on the petrogenesis of Permian-Triassic Emeishan flood basalts in southwestern China. *Lithos* **58**, 145–168.

Xu Y. G., He B., Chung S. L., Menzies M. A. and Frey F. A. (2004) Geologic, geochemical, and geophysical consequences of plume involvement in the Emeishan flood-basalt province. *Geology* **32**, 917–920.

Xu G., Frey F. A., Clague D. A., Weis D. and Beeson M. (2005) East Molokai and other Kea-trend volcanoes: magmatic processes and sources as they migrate away from the Hawaiian hot spot. *Geochem. Geophys. Geosyst.* **6**. http://dx.doi.org/10.1029/2004GC000830.

Xu J. F., Suzuki K., Xu Y. G., Mei H. J. and Li J. (2007a) Os, Pb, and Nd isotope geochemistry of the Permian Emeishan continental flood basalts: insights into the source of a large igneous province. *Geochim. Cosmochim. Acta* **71**, 2104–2119.

Xu Y. G., He B., Huang X. L., Luo Z. Y., Chung S. L., Xiao L., Zhu D., Shao H., Fan W. M., Xu J. F. and Wang Y. J. (2007b) Identification of mantle plumes in the Emeishan Large Igneous Province. *Episodes* **30**, 32–42.

Xu G., Frey F. A., Clague D. A., Abouchami W., Blichert-Toft J., Cousens B. and Weisler M. (2007c) Geochemical characteristics of West Molokai shield and postshield-stage lavas: constraints on Hawaiian plume models. *Geochem. Geophys. Geosyst.* **8**. http://dx.doi.org/10.1029/2006GC001554.

Yamasaki S., Kani T., Hanan B. and Tagami T. (2009) Isotopic geochemistry of Hualalai shield-stage tholeiitic basalts from

submarine North Kona region, Hawaii. *J. Volcanol. Geotherm. Res.* **185**, 223–230.

Yasuda A., Fuji T. and Kurita K. (1994) Melting phase relation of an anhydrous mid-ocean ridge basalt from 3 to 20 GPa: implication for the behavior of subducted oceanic crust in the mantle. *J. Geophys. Res.* **99**, 9401–9414.

Yudovskaya M. A., Kinnaird J. A., Sobolev A. V., Kuzmin D. V., McDonald I. and Wilson A. H. (2013) Petrogenesis of the Lower Zone olivine-rich cumulates beneath the Platreef and their correlation with recognized occurrences in the Bushveld Complex. *Eco. Geol.* **108**, 1923–1952.

Zhang Z. C., Mahoney J. J., Mao J. W. and Wang F. H. (2006) Geochemistry of picritic and associated basalt flows of the western Emeishan flood basalt province, China. *J. Petrol.* **47**, 1997–2019.

Zhang Z. C., Zhi X., Chen L., Saunders A. D. and Reichow M. K. (2008) Re-Os isotopic compositions of picrites from the Emeishan flood basalt province, China. *Earth Planet. Sci. Lett.* **276**, 30–39.

Zhang Z., Mao J., Saunders A. D., Ai Y., Li Y. and Zhao L. (2009) Petrogenetic modeling of three mafic–ultramafic layered intrusions in the Emeishan large igneous province, SW China, based on isotopic and bulk chemical constraints. *Lithos* **113**, 369–392.

Zhang Y., Ren Z. Y. and Xu Y. G. (2013) Sulfur in olivine-hosted melt inclusions from the Emeishan picrites: implications for S degassing and its impact on environment. *J. Geophys. Res.* **118**, 4063–4070.

Zhang L., Ren Z. Y., Nichols A. R. L., Zhang Y. H., Qian S. P. and Liu J. Q. (2014) Lead isotope analysis of melt inclusions by LA-MC-ICP-MS. *J. Anal. Atom. Spectromet.* **29**, 1393–1405.

Zhong Y. T., He B., Mundil R. and Xu Y. G. (2014) CA-TIMS zircon U-Pb dating of felsic ignimbrite from the Binchuan section: implications for the termination age of Emeishan large igneous province. *Lithos* **204**, 14–19.

Zhou M. F., Robinson P. T., Lesher C. M., Keays R. R., Zhang C. J. and Malpas J. (2005) Geochemistry, petrogenesis and metallogenesis of the Panzhihua gabbroic layered intrusion and associated Fe-Ti-V oxide deposits, Sichuan Province, SW China. *J. Petrol.* **46**, 2253–2280.

Zhou M. F., Zhao J. H., Qi L., Su W. C. and Hu R. Z. (2006) Zircon U-Pb geochronology and elemental and Sr-Nd isotopic geochemistry of Permian mafic rocks in the Fuling area, SW China. *Contrib. Mineral. Petrol.* **151**, 1–19.

Zhou M. F., Arndt N. T., Malpas J., Wang C. Y. and Kennedy A. K. (2008) Two magma series and associated ore deposit types in the Permian Emeishan large igneous province, SW China. *Lithos* **103**, 352–368.

Zi J. W., Fan W. M., Wang Y. J., Peng T. P. and Guo F. (2008) Geochemistry and petrogenesis of the Permian mafic dykes in the Panxi region, SW China. *Gondwana Res.* **14**, 368–382.

Associate editor: Fang-Zhen Teng